Structured Discrete Shape Approximation:
Theoretical Complexity and Practical Algorithm

Andreas M. Tillmann[*]   Leif Kobbelt[†]

February 3, 2021

Abstract

We consider the problem of approximating a two-dimensional shape contour (or curve segment) using discrete assembly systems, which allow to build geometric structures based on limited sets of node and edge types subject to edge length and orientation restrictions. We show that already deciding feasibility of such approximation problems is NP-hard, and remains intractable even for very simple setups. We then devise an algorithmic framework that combines shape sampling with exact cardinality minimization to obtain good approximations using few components. As a particular application and showcase example, we discuss approximating shape contours using the classical Zometool construction kit and provide promising computational results, demonstrating that our algorithm is capable of obtaining good shape representations within reasonable time, in spite of the problem's general intractability. We conclude the paper with an outlook on possible extensions of the developed methodology, in particular regarding 3D shape approximation tasks.

1 Introduction and Preliminaries

We are interested in approximately representing two-dimensional shape contours by non-self-intersecting structures that consist of a limited variety of edge and node types which can be connected only in certain finitely many ways. The two main goals of this general task are simplicity of the structure (i.e., using a small number of components) and good approximation quality with respect to the input contour. Aiming at a good trade-off between these conflicting goals gives rise to many possible formulations, e.g., minimizing the number of components while observing a given approximation error tolerance or, conversely, minimizing the approximation error under component budget constraints. Such problem settings are highly relevant in technical applications where scaffolds or custom support structures are built from a small variety of standard beams and connectors in order to reduce fabrication costs ("rationalization"). These structures are often made by assembling sets of (parallel) 2D profiles. This motivates to initially focus on the case of 2D contour approximation; we will remark on possibilities to exploit the methodology introduced here for generalized setups in 2D and 3D in the conclusions.

To set the stage, we define a *discrete assembly system (DAS)* as $\mathcal{G} := (\mathcal{V}, \mathcal{E}, \mathcal{B}, \mathcal{D})$, where $\mathcal{V}$ is a set of *node types* ($n := |\mathcal{V}|$), $\mathcal{E}$ a set of *edge types* ($m := |\mathcal{E}|$), $\mathcal{B} := \{b_e \in \mathbb{Z}_+ : e \in \mathcal{E}\}$ contains (optional) availability *budgets* for each edge type (which may be infinite), and $\mathcal{D} := \{(d_i, V_i, E_i) : V_i \subseteq \mathcal{V}, E_i \subseteq \mathcal{E}, i = 1, \ldots, k\}$ is a collection of k possible *(edge) orientations* d_i (given, e.g., by direction vectors in $\mathbb{R}^2$) along with node types V_i and edge types E_i that are *compatible* with d_i, i.e., to a node $v \in V_i$, an edge $e \in E_i$ can be attached with orientation d_i. (Note that this setup makes the implicit assumption that all nodes of one type have the same orientation in space; in principle, this could be generalized by equipping each V_i with a local coordinate system, but we do not treat such extensions here.) In particular, generally, not every orientation is allowed at every node, and not every edge type is allowed for every orientation.

Formalizing and realizing the vague task of "finding good approximations" of a given shape contour $\mathcal{F} \subset \mathbb{R}^2$ (or curve segment $\mathcal{C}(p_1, p_2) \subset \mathbb{R}^2$ between two points $p_1, p_2 \in \mathbb{R}^2$) by means of a DAS $\mathcal{G}$ poses several challenges. Indeed, to even precisely define a concrete mathematical problem already involves some nontrivial (design) choices. Besides deciding on how to balance the aforementioned two main goals of structural simplicity and approximation quality, one has to choose a measure for the approximation error, deal with the combinatorial "explosion" induced by the discrete setup, and decide on how to handle global positioning and rotation (fixed vs. variable) as well as scaling w.r.t. the input shape. Furthermore, it has to be

---

[*]A. M. Tillmann is with the Institute for Mathematical Optimization, Technische Universität Braunschweig, Germany (e-mail: a.tillmann@tu-bs.de).

[†]L. Kobbelt is with the Visual Computing Institute, RWTH Aachen University, Aachen, Germany (e-mail: kobbelt@cs.rwth-aachen.de)

ensured that the sought DAS construction "follows" the given shape contour (i.e., that it is "$\mathcal{F}$-resembling")
and does not self-intersect in the plane. Moreover, note also that any approximation error induced by a
$\mathcal{G}$-representation of $\mathcal{F}$ or even a single edge cannot be computed without knowing its actual spatial position
(relative to $\mathcal{F}$), which, however, is generally not available a priori.

To nevertheless get a grip on the task, we propose to divide the problem into a "feasibility part" and an
"optimality part". The general idea is to first find an $\mathcal{F}$-resembling $\mathcal{G}$-representation and then rearrange its
edges to reduce the approximation error as far as (locally) possible. To ensure $\mathcal{F}$-resemblance, we sample
the input shape and require the DAS construction to place nodes close to the sample points and to connect
neighboring pairs of those nodes by a $\mathcal{G}$-segment. We call such a DAS construction *feasible* if it adheres to
given type budgets, and we refer to it as *valid* if it additionally corresponds to a non-self-intersecting, or
"planar", structure (i.e., its edges do not overlap or cross one another).

A simple observation is that long $\mathcal{G}$-paths (with many edges, say $m_{\mathcal{G}}$) between two points will ultimately
(for $m_{\mathcal{G}} \to \infty$) deviate strongly from any possible given curve segment between the two points. Moreover,
if the curve segment is relatively straight, it stands to reason that it can be approximated well by a DAS
construction that does not need many struts. Therefore, after sampling the input shape contour, we use the
number of DAS edges between two neighboring nodes as a proxy for the shape approximation error. Relating
the resulting three-phase approach (sampling being phase one) to the two conflicting goals mentioned earlier,
we thus incorporate the goal of simplicity into the second phase by means of minimizing the number of
utilized DAS components (to acquire an $\mathcal{F}$-resembling $\mathcal{G}$-representation), and explicitly address the goal of
low approximation error in the third phase.

The rest of this paper is organized as follows: In the following two subsections, we first discuss related
problems from the literature, and then describe a concrete DAS—the so-called Zometool system—that will
serve as a showcase example throughout the remainder of the paper, and for which we demonstrate with
computational experiments (presented in Section 4) that our method allows to compute good approximations
within reasonable time in practice. We formally define several shape contour approximation and point
connectivity feasibility problems and prove their respective NP-hardness in Section 2, before providing (in
Section 3) a detailed description of the approach that was briefly outlined above. We conclude the paper
with a discussion of some unresolved aspects and possible ways to utilize the methodology developed here for
the even more challenging 3D shape approximation problem, thus providing pointers for interesting future
research.

1.1 Related Work

In the literature, one can find many problems that are in one way or another related to the approximation of
some given shape contour or curve segment between two points by the discrete assembly systems considered
in the present paper. We will briefly outline what appear to be the most closely related works in the following.
Notably, to the best of our knowledge, our key feature of *finitely many edge types/lengths* is missing in all
related previous works, with the exception of those involving Zometool systems (formally described in the
next subsection) or restricted grid-graph settings, and there appears to be no clear way to integrate it into
any of the algorithmic schemes developed therein.

Minimum-Link Paths. Here, the problem is to find a path within a given (often polygonal) shape between
two specified points that uses as few edges as possible (equivalently, the fewest turns). Optimization is
usually done w.r.t. link (edge) number and/or total path length (often Euclidean, but other distance
measures have been considered); see, e.g., [12, 3, 26, 19]. Possible constraints include, in particular,
a discrete set of admissible edge orientations (as in, e.g., [27, 21]), but edges may be arbitrarily long.
Related further problems include ray-shooting variants (turns are restricted to "reflection" at the shape
boundary, cf. [13]), art gallery and watchman route problems, robot motion planning problems (finding
paths that avoid obstacles as in, e.g., [22, 27]) or VLSI routing. A comprehensive overview of minimum-
link path related problems and algorithms is given in the recent survey [18] (and the extensive list of
references therein), see also [6] as a starting point for corresponding path-query problems.

Polygonal Approximation. Here, the problem is often to approximate a given polygon by a "simpler" one,
though other (often convex) shapes are sometimes also considered, and objectives may be minimizing
the enclosed area or the perimeter of the constructed polygonal shape, see, for instance, [10, 24, 20, 1].
As with minimum-link paths, edge type (length) restrictions appear to have not been considered in
this context.

A particular subfield of polygonal approximation that, in fact, includes some problem classes that
are special cases of (certain variants of) the more general problems considered in this paper, is called
schematization. In schematization, the goal is to approximate a given polygon by another in which
all edges are parallel to a given set of orientations/directions (but, generally, not restricted in length),

and the main motivation is to create simplified visually appealing representations largely for use in map-making. Thus, schematization is applied for the development of public transportation route maps (see, e.g., [25, 2]) and in cartography (cf. [17, 5] and references therein), but also in, e.g., handling electromagnetic noise in printed circuit boards [7]. Discretized schematization methods embed the given polygon in a grid graph, wherein the output polygon then corresponds to a selection of edges; see, e.g., [17, 4, 14]. These grid-based problem formulations can be obtained as special cases of our general DAS shape approximation problem by fixing the global positioning and rotation, allowing only edges of a single length per direction (thus yielding the grid graph structure), and focusing on polygonal input shapes. The main approximation error measures considered in discrete schematization are the symmetric difference, the Hausdorff distance, and the (possibly discretized) Fréchet distance. While the special-case relationship provides some useful insights (especially w.r.t. computational complexity, see Section 2), discretized schematization algorithms are inapplicable for the more general DAS problems treated in this paper, since they rely heavily on the grid-graph representation, which is unavailable for general DASs with or without fixed global positioning.

Zometool Shape Approximation. The special DAS case of Zometool systems (cf. Section 1.2 below) and corresponding shape approximation problems in 3D space have been considered in, e.g. [8, 11, 28, 29]. The latter two works use a simulated annealing approach (based on local configuration improvements) to approximate a shape boundary in $\mathbb{R}^3$ that could be adopted to work in two dimensions as well. However, the simulated annealing methodology does not provide any convergence or approximation/optimality guarantees, and may exhibit considerable runtime in practice. These drawbacks partly motivated our developing the method proposed in Section 3, which differs in that it involves high-level heuristic model/design choices—in particular, the sampling phase—but can, in principle, solve the resulting subproblems to global optimality (not restricted to local improvement sequences); moreover, the global positioning of the $\mathcal{G}$-construction is included in the optimization here, but fixed in the simulated annealing approach. We will give some further explanation why simulated annealing would be problematic for the problems considered in the present work after we formally define these problems and describe our novel algorithm, see Section 3.2.3.

Although a future "ultimate" goal is to refine and improve upon solving shape approximation problems in three dimensions, we focus on the 2D case throughout this paper in order to establish theoretical hardness results and a novel algorithmic framework. The former carry over directly to the 3D case, thus settling the open question of computational complexity in that regime as well, while we intend to utilize the latter for handling the 3D setting in future work (see Section 5 for some remarks in that regard). For such an extension, local improvement steps as employed by the simulated annealing algorithm from [28, 29] may become useful as heuristics or solution polishing components.

There exist very many more problems that are in one way or another loosely related to discrete assembly system shape approximation, such as similar path-problems with prescribed angles at the turns or minimizing total turn angle, restrictions to grid-like graph-related structures, curve smoothing approaches, visibility polytopes, or skeleton graph computation. As these are less relevant to the present work, we do not go into more detail here. Similarly, the body of literature on (3D) shape approximation in general is too vast to discuss here, and arguably not directly relevant; also, again, the combined specifics of our DAS seem to set it apart from other approaches.

1.2 The Zometool System

A particular discrete assembly system that exists as a real-world construction kit is the *Zome(tool) system* $\mathcal{Z} := (\mathcal{V}^\mathcal{Z}, \mathcal{E}^\mathcal{Z}, \mathcal{B}^\mathcal{Z}, \mathcal{D}^\mathcal{Z})$, cf., e.g., [11]. Here, we have only one type of nodes, so $n^\mathcal{Z} = |\mathcal{V}^\mathcal{Z}| = 1$; say, $\mathcal{V}^\mathcal{Z} = \{z\}$. This node type is originally defined in 3D, where it has a total of 62 slots at which edges of different types (referred to as *struts* in this context) can be attached – 12 pentagonal slots, into which only red struts fit, 20 triangular slots for yellow struts and 30 rectangular slots for blue struts. The most versatile node type in 2D, derived from the 3D node type by slicing it so that as many slots as possible remain, still has 12 slots (corresponding to orientations in the form of 6 directions and their respective opposites), with 4 struts per color attachable to it in total (2 orientations per color). For each color, three lengths are available (defined as the distance between the midpoints of the two nodes a strut can connect). Thus, in total, there are nine types of struts $\mathcal{E}^\mathcal{Z} = \mathcal{E}_r^\mathcal{Z} \cup \mathcal{E}_y^\mathcal{Z} \cup \mathcal{E}_b^\mathcal{Z}$, with $\mathcal{E}_c^\mathcal{Z} = \{c_1, c_2, c_3\}$ for each color $c \in \mathcal{C} := \{r, y, b\}$ (r for red, y for yellow, b for blue), where w.l.o.g. the length of c_i is smaller than that of c_j whenever $i < j$. In particular, for each strut type, the lengths are related via the golden ratio $\phi := (1+\sqrt{5})/2 \approx 1.618$ as follows: Identifying, for simplicity, each c_i directly with its length (so that $c_1 < c_2 < c_3$ for all $c \in \mathcal{C}$), the medium length is then given as $c_2 = \phi c_1$ and the longest as $c_3 = \phi c_2$. Note that since $\phi^2 = 1 + \phi$, we have $c_3 = c_1 + c_2$. Further nice properties exhibited by the Zome system are node symmetry (i.e., for each slot to plug in a
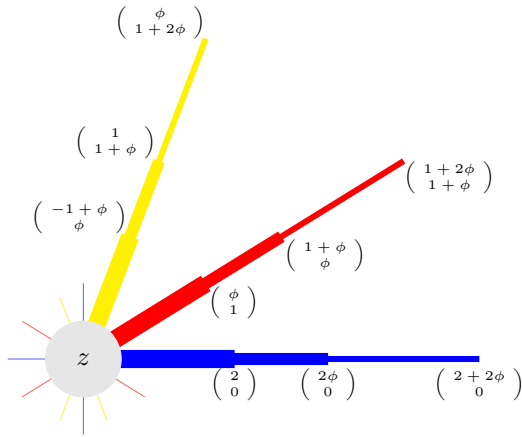
Figure 1: The different Zometool struts and their lengths and orientations (implicitly) in the most versatile two-dimensional Zome system. Strut thicknesses differ for visualization purposes only. Global (node) orientation is $0°$.

strut, there is an opposite slot of the same type in the Zome node z, so for each direction, the opposite direction is also available) and a fixed node orientation (i.e., all nodes have the same orientation in space, defined by any one strut used in the assembled Zome structure). Moreover, assuming w.l.o.g. a scaling such that $b_1 = 2$ and that a Zome node is placed at the origin $(0, 0)$ (or $(0, 0, 0)$ for 3-dimensional setups), the coordinates of each point that can be reached via Zometool components have the form $(\alpha_1 + \phi\beta_1, \alpha_2 + \phi\beta_2)$ (or $(\alpha_1 + \phi\beta_1, \alpha_2 + \phi\beta_2, \alpha_3 + \phi\beta_3)$ in the 3D case), where $\alpha_i, \beta_i \in \mathbb{Z}$ for all $i \in \{1, 2\}$ (or $\{1, 2, 3\}$, respectively). It is worth emphasizing that the listed properties are special to the Zome system and will not (in analogous form) hold for arbitrary DASs in general. However, if we further restrict to a *Zome subsystem* by excluding certain strut lengths and/or types, the properties are retained and, naturally, further structural properties can be observed. Furthermore, note that any Zome path is invariant under permutations of its elements in the sense that the two nodes connected by the path are also connected by all other paths that contain the same struts in an arbitrarily permuted order. (This invariance actually *does* hold for all DASs.)

Based on this scaling ($b_1 = 2$), all other Zome strut lengths are determined as well; Figure 1 provides an overview of the corresponding edge types in the 2D Zome system which offers the largest admissible set of strut orientations. It is worth mentioning that there also exist green Zome struts, leading from the origin to $(2, 2)$, $(2\phi, 2\phi)$ and $(2 + 2\phi, 2 + 2\phi)$, respectively; these are part of an *extended Zome system* which retains the properties of the basic system but naturally allows for even more variety in constructions. Nevertheless, for simplicity, we restrict ourselves to the standard Zome system throughout.

Further details on the Zome system, local configurations and construction examples can be found in [8, 11]; in particular, see also the Zometool shape approximation algorithms based on simulated annealing in [28, 29].

2 Formal Problem Statements and Computational Complexity

In this section, we provide strong intractability results for several essential discrete (2D) shape contour and curve segment approximation problems. In fact, it will turn out that already deciding feasibility is NP-hard, so our complexity results hold regardless of any objective function. Since no theoretically efficient (i.e., polynomial-time) solution methods exists unless P=NP, such intractability results motivate the development of fast heuristics or, possibly, polynomial-time approximation algorithms (with provable guarantees on the solution quality w.r.t. optimality), as well as dedicated exact (but exponential-time) solvers. Thus, ultimately, they provide justification for the mixed-integer programming based approach we propose later (see Section 3) and, retrospectively, also for the simulated annealing heuristic from [28, 29] for (3D) Zometool shape approximation.

2.1 DAS Shape Approximation (Feasibility) Problems

Let us begin with formal definitions of the problems considered here. For simplicity, we state them all as decision problems; corresponding optimization versions can be obtained by asking to optimize some objective function over the set of feasible solutions (in particular, e.g., minimizing some approximate error). To that end, in the following, let $\mathcal{F} \subset \mathbb{R}^2$ be either a *curve segment* (an arbitary curve segment between two distinct points in the plane that does not cross itself) or a *shape contour* (an arbitrary closed curve in the plane that encloses precisely one nonempty connected area). For a point $p \in \mathbb{R}^2$, some nonnegative-definite distance measure $\rho : \mathbb{R}^2 \times \mathbb{R}^2 \to \mathbb{R}_+$ (e.g., the Euclidean ℓ_2-norm difference) and some $\delta \geq 0$, let

$\mathcal{N}_\delta^\rho(p) := \{x \in \mathbb{R}^2 : \rho(x,p) \leq \delta\}$ denote the ρ-ball of radius δ around p.

For a given $\mathcal{G}$ and $\mathcal{F}$, the outcomes we are interested in are always simple paths or cycles[1] constructed from components of $\mathcal{G}$ that (more or less closely) "follow" all of $\mathcal{F}$; for clarity, we shall thus call such paths and cycles *$\mathcal{F}$-resembling $\mathcal{G}$-paths/cycles*, respectively. (Also, recall that such paths/cycles are *valid* only if they are "planar", i.e., without self-intersections, and obey possible edge-type budgets.)

One may think of "following" here as nowhere deviating from $\mathcal{F}$ by more than some constant distance, i.e., being contained in a "corridor" $C_\varepsilon^\sigma(\mathcal{F}) := \{x \in \mathbb{R}^2 : \sigma(x,y) \leq \varepsilon \; \forall y \in \mathcal{F}\} = \{x : x \in \mathcal{N}_\varepsilon^\sigma(y) \text{ for some } y \in \mathcal{F}\}$ for some distance measure σ (possibly different from ρ) and constant $\varepsilon \geq 0$; in case of shape contours, such a corridor should—for a suitable scaling/resolution—generally resemble a "2D torus", i.e., still have a "hole". We note that, here, the corridor definition serves primarily to better describe the notion of following the contour, but otherwise has no direct impact on the main problems under consideration and is not used algorithmically either. Nevertheless, corridor containment could be formally required, as seems common, e.g., in schematization; such requirements lead to variants of our problems of interest, which will be briefly touched upon in the context of computational complexity (Section 2.2).

Rather than via corridor containment constraints, our approach to achieve $\mathcal{F}$-resemblance focusses on sampling the input contour and requiring the $\mathcal{G}$-construction to place DAS nodes in the vicinity of the sampled anchor points and connect each such node to the next—i.e., *in order corresponding to how the sample points occur when traversing $\mathcal{F}$ in a fixed direction (clockwise or counter-clockwise)*—with DAS components. (This will be made precise in the definitions below, though for notational simplicity, we shall assume the sample points are ordered in this fashion, and later implicitly assume this node visitation order when talking about $\mathcal{F}$-resembling $\mathcal{G}$-cycles/paths.)

Our main (decision) problem of interest can be formally stated as follows:

DISCRETE CONTOUR APPROXIMATION WITH SAMPLING (DCA-S): *Given a shape contour $\mathcal{F} \subset \mathbb{R}^2$, ordered sample points $p_1, \ldots, p_k$ on $\mathcal{F}$, a DAS $\mathcal{G} = (\mathcal{V}, \mathcal{E}, \mathcal{B}, \mathcal{D})$, a distance measure $\rho : \mathbb{R}^2 \to \mathbb{R}_+$ and a parameter $\delta \geq 0$, does there exist a valid $\mathcal{F}$-resembling $\mathcal{G}$-cycle with at least one node q_i in each $\mathcal{N}_\delta^\rho(p_i)$, $i \in \{1, \ldots, k\}$, that consists of $\mathcal{G}$-path segments connecting the pairs $(q_1, q_2), (q_2, q_3), \ldots, (q_{k-1}, q_k), (q_k, q_1)$?*

Our computational method (cf. Section 3) will be based on the DCA-S problem. (Indeed, the mixed-integer program we will employ provides a way to answer the above DCA-S problem.) Moreover, the following variant asking for a $\mathcal{G}$-path approximating a curve segment between two distinct points is both of separate interest and will resurface as a subproblem (in a certain sense) in our algorithm.

DISCRETE PATH APPROXIMATION WITH SAMPLING (DPA-S): *Given a curve segment $\mathcal{F} \subset \mathbb{R}^2$ between two points $x_1, x_2 \in \mathbb{R}^2$, a DAS $\mathcal{G} = (\mathcal{V}, \mathcal{E}, \mathcal{B}, \mathcal{D})$, ordered sample points $p_1, \ldots, p_k$ on $\mathcal{F}$, a distance measure $\rho : \mathbb{R}^2 \to \mathbb{R}_+$ and a parameter $\delta \geq 0$, does there exist a valid $\mathcal{F}$-resembling $\mathcal{G}$-path connecting x_1 and x_2 (either directly, or approximately by placing nodes in $\mathcal{N}_\delta^\rho(x_1)$ and $\mathcal{N}_\delta^\rho(x_2)$) with at least one node q_i in each $\mathcal{N}_\delta^\rho(p_i)$, $i \in \{1, \ldots, k\}$, that consists of $\mathcal{G}$-path segments connecting the pairs $(q_1, q_2), (q_2, q_3), \ldots, (q_{k-1}, q_k)$?*

In fact, the feasibility of *freely* connecting two distinct points in $\mathbb{R}^2$ (without regard to any curve segment resemblance objectives, sample points or corridor containment) using components of a DAS is still of interest as an intuitively simpler-seeming, very basic problem:

DISCRETE POINT CONNECTIVITY (DPC): *Given two points $x_1, x_2 \in \mathbb{R}^2$ and a DAS $\mathcal{G}$, can x_1 and x_2 be connected by a valid $\mathcal{G}$-path?*

2.2 Intractability Results

We now turn to the computational complexity of the fundamental DAS shape approximation problems defined above. Before providing our novel results, we point out that the connection to discrete schematization discussed in Section 1.1 allows to directly infer hardness results for some special cases of our DAS problems. More precisely, suppose that, in our setting, we do *not* use sample points, that the global position of the sought $\mathcal{G}$-cycle is fixed, and that only horizontal and vertical edges of the same unit length are available. The position fixing and available edge types imply that the $\mathcal{G}$-cycle is, in fact, a (simple) cycle in a grid graph that "overlays" the given shape contour $\mathcal{F}$. Now, [14, Thm. 1] states that, even for a simple polygon $\mathcal{F}$, it is NP-complete to decide whether this grid graph contains a ($\mathcal{G}$-)cycle with Fréchet distance no larger than a given $\epsilon > 0$. The Fréchet distance (see, e.g., [14] for a precise definition) takes the place of an approximation error measure to quantify shape resemblance; using the symmetric difference (the total area of those parts of the union of two shapes that are contained in only one of them) leads to a similar NP-hardness results, see [14, Thm. 2]. When a corridor is defined in terms of Hausdorff distances, [4, Thm. 1] gives NP-hardness of an analogous grid-graph/polygon DAS variant.

---

[1]Here, we appropriate some terminology from graph theory, but note that, while structurally similar to (planar) graphs, concrete $\mathcal{G}$-constructions are essentially *defined* via their embedding in the plane, whereas graphs are more abstract objects that may or may not have planar embeddings.
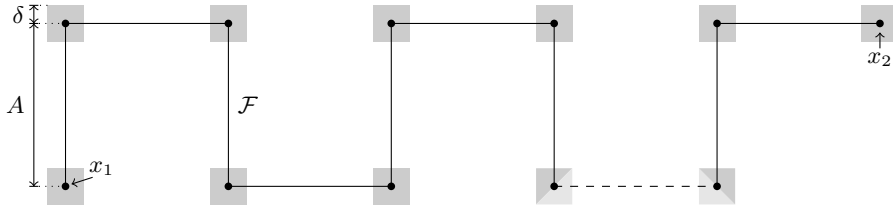
Figure 2: Schematic illustration of the construction from the proof of Theorem 2.1: The neighborhoods $\mathcal{N}_\delta^\rho(p_i)$ (shaded boxes) contain all points with ℓ_∞-norm distance at most δ from the associated sample points p_i (black dots), respectively. The piecewise linear x_1-x_2-path $\mathcal{F}$ is the solid curve (with turns at $p_1, \ldots, p_{m-1}$); all m segments of this path have length A. The dashed and lighter-shaded parts of $\mathcal{F}$ and some $\mathcal{N}_\delta^\rho(p_i)$, respectively, illustrate a continuation of the discernible pattern in accordance with the actual instance size.

Thus, if we replace the sample-point part in DCA-S by corridor containment requirements, and restrict further to a fixed global positioning and grid-inducing DASs, the abovementioned results can indeed be seen as special cases, and consequently, the NP-hardness results carry over. Nevertheless, these special cases are not precisely what we are interested in here: We explicitly do *not* want to fix the global positioning a priori, and we intend to work with a DAS that does *not* induce a grid-like graph (such as the Zome system described in Section 1.2). Furthermore, the requirement to place nodes in sample point neighborhoods is weaker than requiring the full graph to lie within a certain distance of the given shape contour (or curve segment). Therefore, while no doubt closely related, the hardness results described above do not precisely match our setting. While it may be possible to extend the rather complicated reductions from [14, 4] to analogous DPA-S variants and/or modify the corridor containment there by a requirement to have the sought cycle traverse sample point neighborhoods, the novel proofs we provide below are also significantly simpler.

Our intractability results will be based on the following two problems, which are well-known to be NP-complete (see [9, problems SP12 and SP15]):

PARTITION: *Given positive integers $a_1, \ldots, a_n$, does there exist a subset I' of $I := [n] := \{1, \ldots, n\}$ such that $\sum_{i \in I'} a_i = \sum_{i \in I \setminus I'} a_i$?*

3-PARTITION: *Given positive integers $a_1, \ldots, a_{3m}$ and A such that $A/4 < a_i < A/2$ for all $i \in I := [3m]$ and $\sum_{i \in I} a_i = mA$, can I be partitioned into m disjoint (3-element) sets $I_1, \ldots, I_m$ such that, for all $j \in \{1, \ldots, m\}$, $\sum_{i \in I_j} a_j = A$?*

Our first result is about DPA-S; the subsequent ones about the other problems are derived along the same lines, with slight variations of the same main proof idea.

Theorem 2.1. *The DPA-S problem is NP-hard in the strong sense, even restricted to piecewise linear curve segments $\mathcal{F}$ with right-angle turns and integral-coordinate turning points and end points (x_1, x_2), integral-coordinate sample points, square (ℓ_∞-norm) boxes as sample point neighborhoods $\mathcal{N}_\delta^\rho(\cdot)$, and DASs $\mathcal{G}$ with only one node type, horizontal and vertical orientations, and integral-length edge types.*

Proof. We reduce from 3-PARTITION: Let $(a_1, \ldots, a_{3m}, A)$ be a given 3-PARTITION instance; we may and do assume that A is polynomially bounded my m, since [9] proved that 3-PARTITION remains NP-complete under these restrictions and is thus, in fact, NP-complete *in the strong sense*[2]. We construct an instance of DCA-S with restrictions as specified in the theorem statement: Let k be the number of *distinct* a_i-values in the given 3-PARTITION instance and associate with each such value (say, a_ℓ') an edge type e_ℓ with length a_ℓ'; set $\mathcal{E} := \{e_\ell : \ell = 1, \ldots, k\}$ and define the budgets $\mathcal{B} := \{b_e : e \in \mathcal{E}\}$ with $b_{e_\ell} := |\{i \in [3m] : a_i = a_\ell'\}|$. Further, let $\mathcal{V} := \{v\}$ (the single node type), and let $\mathcal{D}$ be given via the horizontal and vertical direction vectors, all of which are defined to be compatible with each node and edge type, i.e., $\mathcal{D} := \{(d, \mathcal{V}, \mathcal{E}) : d \in \{\pm(1,0), \pm(0,1)\}\}$. This completes the (obviously polynomial) construction of the DAS $\mathcal{G} := (\mathcal{V}, \mathcal{E}, \mathcal{B}, \mathcal{D})$. To specify the curve segment, sample points and their neighborhoods, let $0 \le \delta < A/4$ (say, $\delta := A/9$), $\rho(x, y) := \|x - y\|_\infty$, and define points $p_j := (\lfloor j/2 \rfloor A, (\lceil j/2 \rceil \mod 2)A)$ for $j = 0, 1, \ldots, m$. Set $x_1 := p_0$, $x_2 := p_m$ and define $\mathcal{F}$ to be the chain of piecewise linear segments connecting p_j with p_{j+1} for all $j = 0, \ldots, m-1$ (i.e., $\mathcal{F} := \bigcup_{i \in [m]} \{\lambda p_{i-1} + (1-\lambda)p_i : \lambda \in [0,1]\}$), see Figure 2 for a visualization. Clearly, by means of p_j, ρ and δ, both $\mathcal{F}$ and each $\mathcal{N}_\delta^\rho(p_i)$ can be encoded with size polynomial in that of the given 3-PARTITION instance, and containment in either can be evaluated in polynomial time.

Thus, the overall construction is indeed polynomial, so it remains to show that the given 3-PARTITION instance has a positive answer if and only if the constructed DPA-S instance does as well:

---

[2]Recall that this means that, unless P=NP, not only does there not exist a polynomial algorithm to decide the problem, but also no pseudo-polynomial algorithm (and, for strongly NP-hard *optimization* problems, no fully polynomial-time approximation scheme (FPTAS)). We refer to [9] for details.

"⇒": If $(a_1, \ldots, a_{3m}, A)$ is a "yes"-instance of 3-PARTITION with certificate $(I_1, \ldots, I_m)$, a corresponding solution to the DPA-S instance is given by the valid $\mathcal{F}$-resembling $\mathcal{G}$-path that connects x_1 and x_2 by using (exactly) three edges to reach each respective next (right-angle) turn, thus mapping $I_1, \ldots, I_m$ to the m path segments of length A. Clearly, all direction constraints are obeyed, the budgets are sufficient (in fact, depleted with no left-overs) and the $\mathcal{G}$-path precisely overlays $\mathcal{F}$ (thus placing DAS-nodes at each turning/sample point, so each $\mathcal{N}_\delta^\rho(p_i)$ indeed contains a node). Thus, this solution shows that the DPA-S instance has a "yes" answer.

"⇐": Conversely, let a "yes"-certificate of the DPA-S instance be given, and let $e_1, \ldots, e_M$ be the sequence of edge types used along the $\mathcal{G}$-path from x_1 to x_2. Since $\delta < A/4 < \min a_i'$ and $\max a_i' < A/2$, exactly three edges of the same orientation must be used in each path-segment. Moreover, the lengths of all these three-edge subsets must sum to A, because otherwise, a neighborhood $(\mathcal{N}_\delta^\rho(p_i)$-) containment condition would be violated either immediately or after the next turn (recall also that the neighborhoods are traversed according to a given order). This shows that $M = 3m$, and that we can construct a "yes"-certificate $I_1, \ldots, I_m$ for the input 3-PARTITION instance by traversing $e_1, \ldots, e_{3m}$ and mapping the encountered three-tuples $E_j := (e_{3j-2}, e_{3j-1}, e_{3j})$, $j = 1, \ldots, m$, to $I_j := \{j_1, j_2, j_3\}$ with $j_1 := \min\{i : a_i = a_{3j-2}', i \notin I_k \; \forall k < j\}$, $j_2 := \min\{i : a_i = a_{3j-1}', i \notin I_k \; \forall k < j, i \neq j_1\}$, and $j_3 := \min\{i : a_i = a_{3j}', i \notin I_k \; \forall k < j, i \neq j_1, i \neq j_2\}$, respectively.

This proves NP-hardness of the DPA-S problem. Moreover, in particular, for the DPA-S instance constructed from the 3-PARTITION input with the stated restrictions, all encoding lengths as well as the occurring numbers themselves are polynomially bounded by the instance *size* (number of specified integers, $\mathcal{O}(m)$) alone. Therefore, the "strong sense" assertion of NP-hardness carries over to DPA-S as well.

Finally, note that the above proof goes through completely analogously if we require DAS nodes exactly at x_1 and x_2, so both variants from the DPA-S definition are covered. $\qquad\square$

It is easily seen that the proof of Theorem 2.1 goes through completely analogously for DPA-S variants requiring the $\mathcal{G}$-path to be contained in a corridor $\mathcal{C}_\varepsilon^\sigma(\mathcal{F})$ and/or minimizing a (nonnegative definite) error measure w.r.t. $\mathcal{F}$. Thus, we immediately obtain the following.

Corollary 2.2. *The DPA-S problem remains* NP-*hard in the strong sense (under the same restrictions as listed in Theorem 2.1) if the $\mathcal{F}$-resembling $\mathcal{G}$-path P is required to lie within a corridor $\mathcal{C}_\varepsilon^\sigma(\mathcal{F})$ around $\mathcal{F}$ and/or the objective of minimizing an approximation error $\alpha(P, \mathcal{F}) \geq 0$ is included. In the latter case, hardness persists even if no sample point neighborhood (and/or corridor) containment is required.*

Proof. We can directly extend the reduction from the proof of Theorem 2.1 by letting (for instance) $\mathcal{C}_\varepsilon^\sigma(\mathcal{F}) := \{x : \|x - y\|_\infty \leq \delta \; \forall y \in \mathcal{F}\}$ and observing that any nonnegative definite error measure (e.g., the area between $\mathcal{F}$ and the $\mathcal{G}$-path P, or an arbitrary metric) achieves minimum value $\alpha(P, \mathcal{F}) = 0$ if and only if P exactly matches $\mathcal{F}$. $\qquad\square$

Note that as a particular consequence, testing whether the input is already within (i.e., can be exactly overlayed by a construction from) the budgeted DAS system is already NP-hard. (This can be seen by considering DPA-S without sample point or corridor requirement and the objective of minimizing the approximation error defined, e.g., via the discrete metric $\alpha(p, q) = 0$ if $p = q$, and 1 otherwise.)

Remark 2.3. *It is not immediately clear whether the DPA-S decision problem is contained in* NP. *For this to hold, we would need to assert that a "yes"-certificate for an (arbitrary) DPA-S instance has encoding length polynomially bounded by that of the instance, and that all constraints can be verified in polynomial time. Allowing only rational input data (in particular, edge lengths and point coordinates) and suitably "simple" definitions of $\mathcal{F}$ and $\mathcal{N}_\delta^\rho(p_i)$ (and $\mathcal{C}_\varepsilon^\sigma(\mathcal{F})$ and/or $\alpha(P, \mathcal{F})$, in the variants from Corollary 2.2), containment in* NP *may appear to be easy to demonstrate. For the variant that places DAS nodes exactly at $x_1, x_2 \in \mathbb{Q}^2$, restricting to piecewise linear $\mathcal{F}$ with rational turn points and neighborhoods based on, say, ℓ_1- or ℓ_∞-norm differences (such as used in the reduction above), containment in* NP *is indeed obtained straightforwardly, making the problem* NP-*complete (in the strong sense). However, allowing the end nodes of the $\mathcal{G}$-path to deviate from x_1 and x_2, respectively, a certificate might be a valid $\mathcal{F}$-resembling $\mathcal{G}$-cycle that involves node coordinates of non-polynomial encoding length (e.g., irrational values), so containment in* NP *cannot be proven in general. Analogous arguments hold for the other problems discussed below (DCA-S, DPC) as well; for brevity, we mention this only once here.*

The above results extend straightforwardly to the DCA-S problem (and corresponding variants):

Theorem 2.4. *The DCA-S problem is* NP-*hard in the strong sense, even restricted to piecewise linear curve segments $\mathcal{F}$ with right-angle turns and integral-coordinate turning and sample points, square (ℓ_∞-norm) boxes as sample point neighborhoods $\mathcal{N}_\delta^\rho(\cdot)$, and DASs $\mathcal{G}$ with only one node type, horizontal and vertical orientations, and integral-length edge types.*
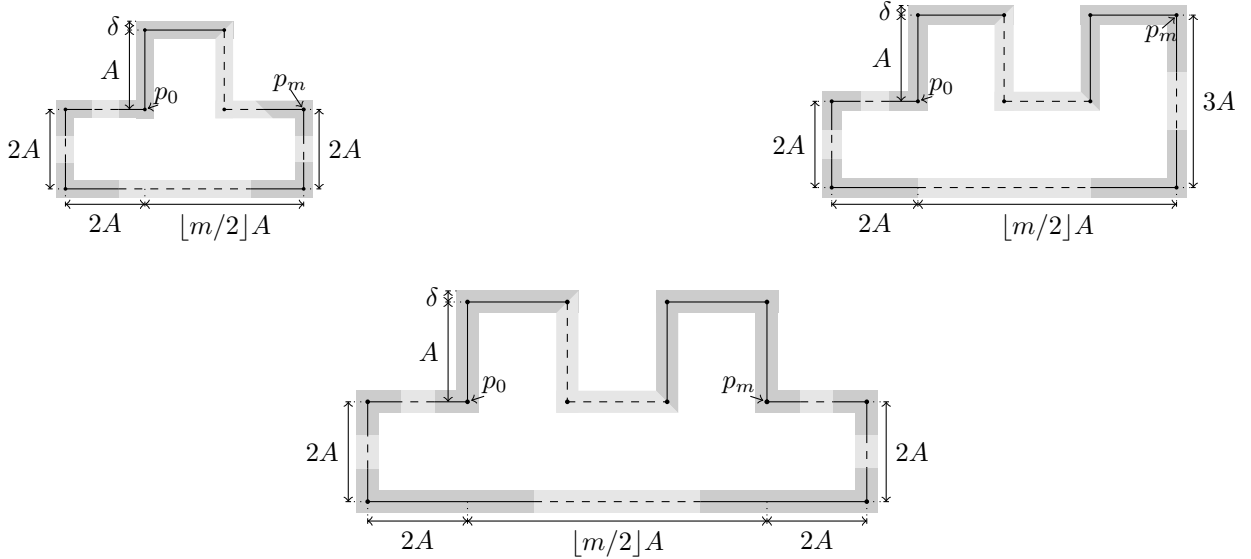
Figure 3: Schematic illustration of the construction from the proof of Theorem 2.4 (and Corollary 2.6) in the cases m and $\lceil m/2 \rceil$ even (top left), m even and $\lceil m/2 \rceil$ odd (top right), or m odd (bottom): The corridor $C_\delta^\rho(\mathcal{F})$ (shaded region) contains all points with ℓ_∞-norm distance at most δ from the piecewise linear shape contour $\mathcal{F}$ (solid curve). All m segments of the path p_0-p_1-$\cdots$-p_m have length A; the corridor is 2δ wide. The dashed and lighter-shaded parts of $\mathcal{F}$ and $C_\delta^\rho(\mathcal{F})$, respectively, illustrate a continuation of the discernible pattern (or of long auxiliary segments) in accordance with the actual instance size.

Proof. We modify the reduction used to show NP-hardness of the DPA-S problem, so at first, let $\mathcal{V}$, $\mathcal{E}$, $\mathcal{D}$ and $\mathcal{B}$ as well as k, ρ, δ and $p_0, \ldots, p_m$ be constructed from a given 3-PARTITION instance as in the proof of Theorem 2.1. Depending on whether m and $\lceil m/2 \rceil$ are even or odd, we construct further points (in order to specify $\mathcal{F}$ and to choose as sample points) and add edge types as follows:

- If m is odd (so $\lceil m/2 \rceil$ is always even and $p_m = (\lfloor m/2 \rfloor A, 0)$, $p_{m-1} = (\lfloor (m-1)/2 \rfloor A, A) = (\lfloor m/2 \rfloor A, A))$, define $p_{m+1} := ((\lfloor m/2 \rfloor + 2)A, 0)$, $p_{m+2} := ((\lfloor m/2 \rfloor + 2)A, -2A)$, $p_{m+3} := (-2A, -2A)$ and $p_{m+4} := (-2A, 0)$, and add edge type e_{k+1} with length $(\lfloor m/2 \rfloor + 4)A$, budget $b_{e_{k+1}} = 1$ and compatible directions $\pm(1, 0)$, as well as edge type e_{k+2} with length $2A$, budget $b_{e_{k+2}} = 4$ and compatible directions $\{\pm(0, 1), \pm(1, 0)\}$.

- If both m and $\lceil m/2 \rceil$ are even (so $\lceil m/2 \rceil = m/2 = \lfloor m/2 \rfloor$, $p_m = ((m/2)A, 0)$ and $p_{m-1} = (\lfloor (m-1)/2 \rfloor A, (\lceil (m-1)/2 \rceil \mod 2)A) = ((m/2-1)A, 0))$, define $p_{m+1} := (\lfloor m/2 \rfloor A, -2A)$, $p_{m+2} := (-2A, -2A)$ and $p_{m+3} := (-2A, 0)$, and add edge type e_{k+1} with length $(\lfloor m/2 \rfloor + 2)A$, budget $b_{e_{k+1}} = 1$ and compatible directions $\pm(1, 0)$, as well as edge type e_{k+2} with length $2A$, budget $b_{e_{k+2}} = 3$ and compatible directions $\{\pm(0, 1), \pm(1, 0)\}$.

- In the final case, m is even and $\lceil m/2 \rceil = m/2 = \lfloor m/2 \rfloor$ is odd (so $p_m = ((m/2)A, A)$ and $p_{m-1} = ((m/2-1)A, A))$; then, we define $p_{m+1} := (\lfloor m/2 \rfloor A, -2A)$, $p_{m+2} := (-2A, -2A)$ and $p_{m+3} := (-2A, 0)$, and add edge type e_{k+1} with length $(\lfloor m/2 \rfloor + 2)A$, budget $b_{e_{k+1}} = 1$ and compatible directions $\pm(1, 0)$, as well as edge types e_{k+2} and e_{k+3} with lengths $3A$ and $2A$, budgets $b_{e_{k+2}} = 1$ and $b_{e_{k+3}} = 2$ and compatible directions $\pm(0, 1)$ and $\{\pm(0, 1), \pm(1, 0)\}$, respectively.

Finally, define the shape contour $\mathcal{F}$ as the piecewise-linear cycle $p_0 \to p_1 \to \cdots \to p_{m+3} (\to p_{m+4}) \to p_0$. Figure 3 illustrates the construction for the three cases (for the DCA-S variant with a feasible corridor of ℓ_∞-width δ).

It is now easily seen, analogously to the proof of Theorem 2.1, that a solution to a "yes"-instance of 3-PARTITION is in one-to-one correspondence with (the core part of) that of a "yes"-instance of the constructed DCA-S instance (in any case); in particular, the additional edge types serve simply to "close the loop" and cannot be used in any other parts of the $\mathcal{G}$-cycle (note that, since $\delta < A/4$, $\lfloor m/2 \rfloor A \geq 3A > 2A > A + 2\delta$, so even the shortest new edge does not fit anywhere else except in the accordingly designed new segments). Thus, the previously crucial problem of connecting p_0 and p_m by a valid $\mathcal{G}$-path is subsumed by that of finding a valid $\mathcal{F}$-resembling $\mathcal{G}$-cycle here. (Unlike in the fixed end-point variant of DPA-S, here, a feasible DCA-S solution never needs to overlay $\mathcal{F}$ exactly, but due to the choice of δ, there still can be only exactly three edges of type e_ℓ, $\ell \in [k]$, per segment of the shape contour subpath from p_0 to p_m.) Furthermore, since the previous construction was only modified by adding a constant number of new polynomially-bounded

8

elements but is otherwise completely analogous, it can be carried out in polynomial time with all occurring numbers and their encoding lengths being polynomially bounded by the instance size (i.e., polynomial in m). Thus, the above extended reduction proves NP-hardness in the strong sense of the DCA-S problem. $\square$

Remark 2.5. *In the above proof of Theorem 2.4, the budget constraints for auxiliary edges added to the original construction are not essential and could just as well be omitted (i.e., using infinite budgets).*

Analogously to the corresponding results for DPA-S, we immediately also obtain intractability of the DCA-S variants involving a feasible corridor (cf. Figure 3) and/or approximation error minimization:

Corollary 2.6. *The DCA-S problem is NP-hard in the strong sense (under the same restrictions as listed in Theorem 2.4) if the $\mathcal{F}$-resembling $\mathcal{G}$-cycle C is required to lie within a corridor $C_\varepsilon^\sigma(\mathcal{F})$ around $\mathcal{F}$ and/or the objective of minimizing an approximation error $\alpha(C, \mathcal{F}) \geq 0$ is included. In the latter case, hardness persists even if no sample point neighborhood (and/or corridor) containment is required.*

Proof. We can extend the proof of Theorem 2.4 along the same lines as in that of Corollary 2.2. $\square$

A more basic problem simply asks whether a given DAS allows to connect two given points in the plane, without asking for any resemblance to some curve segment or shape contour. This is precisely the DPC problem defined earlier; as it turns out, even this fundamental problem is already (weakly) NP-hard.

Theorem 2.7. *The DPC problem is NP-hard, even if restricting the DAS to one node type, horizontal and vertical orientations, and integral-length edge types. For rational input, DPC is contained in NP (and thus NP-complete).*

Proof. We now reduce from PARTITION, which is a weakly NP-hard problem [9]. Given an instance $(a_1, \ldots, a_n)$ of PARTITION, let $A := \frac{1}{2} \sum_{i=1}^n a_i$ and construct an instance of DPC as follows (along the same lines as in the previous proof for DPA-S): Let k be the number of distinct a_i-values and associate with each such value (say, a_ℓ') an edge type e_ℓ with length a_ℓ' to obtain $\mathcal{E} := \{e_\ell : \ell = 1, \ldots, k\}$ and budgets $\mathcal{B} := \{b_e : e \in \mathcal{E}\}$, where $b_{e_\ell} := |\{i \in [3m] : a_i = a_\ell'\}|$. We again use a single node type $\mathcal{V} := \{v\}$ and let $\mathcal{D} := \{(d, \mathcal{V}, \mathcal{E}) : d \in \{\pm(1,0), \pm(0,1)\}\}$, i.e., the horizontal and vertical directions are to be compatible with each node and edge type. This defines the DAS $\mathcal{G} := (\mathcal{V}, \mathcal{E}, \mathcal{B}, \mathcal{D})$. Finally, we set $x_1 := (0,0)$ and $x_2 := (A, A)$. Clearly this construction can be carried out in polynomial time and space.

It remains to demonstrate that the given PARTITION instance has a "yes"-answer if and only if the constructed DPC instance does. To that end, note that there is a one-to-one correspondence between a partition $I', [n] \setminus I'$ such that $\sum_{i \in I'} a_i = \sum_{i \notin I} a_i (= A)$ and the edges with horizontal or vertical orientation, respectively: To connect x_1 and x_2, we need to "go" A in both directions, which is possible if and only if the total of n edges can be partitioned into vertical and horizontal edges with respective length sums A.

While this shows NP-hardness of DPC, when restricting to rational input (coordinates, orientations and edge lengths), containment in NP is obvious, proving the second claim and thus completing the proof. $\square$

The above result has several consequences that may be of further, separate interest:

Corollary 2.8. *Given a DAS $\mathcal{G}$ and two points $x_1, x_2 \in \mathbb{R}^2$, it is NP-hard to find a shortest valid $\mathcal{G}$-path connecting x_1 and x_2, i.e., one with the smallest number of edges.*

Proof. The proof of Theorem 2.7 can be directly adapted to the corresponding decision problem "Given $\mathcal{G}$, x_1, x_2 and a positive integer k, can x_1 and x_2 be connected by a valid $\mathcal{G}$-path using at most k edges?", by letting $k := n$ (the number of elements of the original input PARTITION instance). $\square$

Furthermore, we could reintroduce a curve segment and sample points (and/or a feasible corridor) into the DPC problem and the proof of Theorem 2.7, thereby obtaining another proof of NP-hardness for the DPA-S problem. Although Theorem 2.1 gives a stronger result than a reduction from PARTITION, this alternative proof shows that the DPA-S problem and its variants (from Corollary 2.2) still remain (weakly) NP-hard *even if the curve segment to be approximated is piecewise linear with a single right-angle turn*. Moreover, similarly extending the construction along the same lines as in the proof of Theorem 2.4, we also obtain that the DCA-S variants remain (weakly) NP-hard *even when restricted to simple square shapes*. We omit the straightforward details of the constructions, which mirror that in the previous proofs (cf. Figures 2 and 3, in particular).

In the remainder of the paper, we will demonstrate that in spite of the theoretical intractability, good solutions to the DAS shape contour approximation problems can be obtained in practice within reasonable time. For simplicity, we will mostly restrict our discussion to the contour approximation problem (DCA-S) and omit an explicit treatment of the curve segment approximation task (DPA-S). Indeed, it is straightfoward to adapt the developed approaches and methods to the DPA-S problem.

3 Methodology & Algorithm

Computing a "best" $\mathcal{F}$-resembling $\mathcal{G}$-cycle (w.r.t. some quality measure) is clearly a non-trivial task posing many challenges, as outlined in the introduction. Aside from the theoretical intractability of even deciding feasibility established in the previous section, evaluating error measures is generally not possible without knowing the actual $\mathcal{G}$-cycle and therefore hard to directly incorporate into an optimization scheme.

In our general setting, graph-based methods (such as those working on grid-graphs found in the schematization context, cf., e.g., [17, 4]) are inadequate since it is not known (or computationally infeasible to set up) a priori where possible struts may be located, and location is crucial for assigning weights that reflect closeness to $\mathcal{F}$. Indeed, the shape similarity of two contours is not trivial to formalize. From a perceptual point of view, distance, relative orientation, and even curvature distribution would have to be taken into account, which is quite difficult in our DAS setting with discrete strut lengths and orientations. For simplicity, we therefore resort to a purely distance-based metric and leave generalizations to future work. However, pure max-norms such as the Hausdorff-distance or the Fréchet-distance are not well-suited for our purposes since they would only provide guidance for the optimization in those regions of the contour where the deviation is maximal while changes in other regions of the contour do not affect the metric at all. Thus, we have to find a well-balanced compromise between a prescribed (desired) maximum approximation tolerance and an averaged deviation norm that minimizes, or allows to control, the distance everywhere regardless of the global tolerance threshold.

We find this compromise in the following way: We propose a three-phase approach that first obtains a set of sample points along $\mathcal{F}$, then solves a mixed-integer program (MIP) to obtain a solution to a DCA-S problem with minimal number of struts, and finally explores the possible arrangements of the selected struts in order to find the best approximation to $\mathcal{F}$ that can be constructed using them. For the DCA-S subproblem, we prescribe a "global" desired approximation tolerance δ and, by solving a MIP in the second stage, then find a set of points q_i which lie within a δ-neighborhood of the sample points and which can be connected (in a given order) by $\mathcal{G}$-path segments that form a $\mathcal{G}$-cycle. In the final stage of the algorithm we then compute, for each segment, the permutation of the struts of that segment that leads to the minimal averaged deviation, i.e., to the minimal area between the two contours ($\mathcal{F}$ and the computed $\mathcal{G}$-cycle). This third stage is, of course, not guaranteed to actually respect the desired tolerance δ (except around the sampled points), but it usually provides good shape similarity if the anchor points were chosen such that the contour segments between them are sufficiently simple (i.e., relatively straight).

Focussing on $\mathcal{G}$-paths (between regions around the sample points) with small number of struts avoids the problem of inaccessibility of suitable placement-dependent strut/path-quality measures on the one hand, and on the other hand, quite intuitively implements the fact that desirable solutions will not stray too far from $\mathcal{F}$ (or contain odd zigzagging parts) and hence necessarily have relatively few struts. It also makes edge-crossings/overlaps less likely – although we do not explicitly enforce this planarity of the sought $\mathcal{G}$-paths or cycles; it turned out to be very often fulfilled automatically in our experiments, and can probably often easily be remedied by postprocessing in practice[3]. Once the number of struts is known (for each segment of the $\mathcal{G}$-cycle to be computed), we can exploit the fact that struts in a $\mathcal{G}$-path can be arbitrarily permuted without disconnecting the end points, and simply enumerate all such permutations and evaluate the above-mentioned averaged deviation approximation error to $\mathcal{F}$ for each one in order to identify the best arrangement using the computed strut collection. (Should full enumeration become too expensive, which may happen if a segment contains many struts, one may also resort to a greedy construction that determines a permutation by sequentially picking locally optimal struts.)

In the remainder of this section, we will first introduce mixed-integer programming (MIP) formulations for some of the DAS shape approximation problems, and then describe in detail the overall algorithm to compute $\mathcal{F}$-resembling $\mathcal{G}$-cycles of high quality. In order to avoid repetitions when turning to computational experiments later, we directly discuss the MIPs and algorithms in the context of *Zometool* shape approximation; thus, $\mathcal{G}$ will henceforth always refer to the (standard) Zometool system described in the introduction (see Section 1.2). This concretization notwithstanding, we emphasize that all ingredients straightforwardly generalize to arbitrary other DASs.

3.1 MIP Formulations

Recall from the introduction that, assuming a Zometool node is placed at the origin $(0,0)$ and that the shortest blue strut length is scaled to $b_1 = 2$, every point reachable by Zometool components has coordinates of the form $(\alpha_1 + \phi\beta_1, \alpha_2 + \phi\beta_2)$ with $\alpha_i, \beta_i \in \mathbb{Z}$ for $i = 1, 2$. For every different strut in the Zometool

---

[3]It must be noted that there may be instances for which solution self-intersection issues *cannot* be fixed at all. This is more likely to occur if the resolution is too low, i.e., struts are quite long compared to the overall global scale of the input. At higher resolutions, this should no longer be problematic, by virtue of minimizing the number of struts per segment. Unfortunately, an adequate choice of scale/resolution is not always clear a priori.

system, there are four admissible directions, cf. Figure 1, where two of them are the respective opposites of the other two. Thus, for each strut color $e \in \{b, r, y\}$ (blue, red, yellow) and length $i \in \{s, m, \ell\}$ (short, medium, long), we may collect the corresponding translation vectors as columns of the following matrices:

$$M_s^b = \begin{pmatrix} 2 & 0 \\ 0 & 2 \end{pmatrix}, \qquad\qquad M_m^b = \begin{pmatrix} 2\phi & 0 \\ 0 & 2\phi \end{pmatrix},$$

$$M_\ell^b = \begin{pmatrix} 2 + 2\phi & 0 \\ 0 & 2 + 2\phi \end{pmatrix},$$

$$M_s^r = \begin{pmatrix} \phi & \phi \\ -1 & 1 \end{pmatrix}, \qquad\qquad M_m^r = \begin{pmatrix} 1 + \phi & 1 + \phi \\ -\phi & \phi \end{pmatrix},$$

$$M_\ell^r = \begin{pmatrix} 1 + 2\phi & 1 + 2\phi \\ -1 - \phi & 1 + \phi \end{pmatrix},$$

$$M_s^y = \begin{pmatrix} -1 + \phi & -1 + \phi \\ -\phi & \phi \end{pmatrix}, \qquad\qquad M_m^y = \begin{pmatrix} 1 & 1 \\ -1 - \phi & 1 + \phi \end{pmatrix},$$

$$M_\ell^y = \begin{pmatrix} \phi & \phi \\ -1 - 2\phi & 1 + 2\phi \end{pmatrix}.$$

For example, starting at a node (x, y), taking a "step" along a strut e of length i in positive or negative/opposite direction of, say, the second orientation thus leads to target node coordinates $(x + (M_i^e)_{12}, y + (M_i^e)_{22})$ or $(x - (M_i^e)_{12}, y - (M_i^e)_{22})$, respectively.

3.1.1 Connecting Points by Zome-Paths

Now, let us first consider the (Zome-)DPC problem: Can we connect two given points $x_1, x_2 \in \mathbb{R}^2$ by a $\mathcal{G}$-path? This question can be answered by solving the following integer feasibility problem (IFP):

$$\begin{aligned} \text{find} \quad & \gamma_{e,i}^+, \gamma_{e,i}^- \in \mathbb{Z}_+^2 \quad \forall e \in \{b, r, y\}, i \in \{s, m, \ell\} \\ \text{s.t.} \quad & x_2 = x_1 + \sum_{e \in \{b,r,y\}} \sum_{i \in \{s,m,\ell\}} M_i^e \left(\gamma_{e,i}^+ - \gamma_{e,i}^- \right) \\ & \left((\gamma_{e,i}^+)_j \cdot (\gamma_{e,i}^-)_j = 0 \quad \forall e \in \{b, r, y\}, i \in \{s, m, \ell\}, j \in \{1, 2\} \right) \end{aligned} \tag{1}$$

Here, for each $e \in \{b, r, y\}$ and $i \in \{s, m, \ell\}$, the variables $(\gamma_{e,i}^+)_j \in \mathbb{Z}_+$ and $(\gamma_{e,i}^-)_j \in \mathbb{Z}_+$ specify the number of times the j-th corresponding strut (i.e., the j-th column vector of matrix M_i^e) is used in positive direction (directly as given in M_i^e, superscript "+") or in negative direction (superscript "−"), respectively. The equality constraint models the desired connectivity by expressing point x_2 as x_1 plus an integer linear combination of the available struts. Thus, the DPC question can be answered in the affirmative if and only if a feasible variable assignment for the above IFP can be found. The last, optional complementarity constraint may be used to exclude paths that contain segments of same-color same-length struts being used in opposite directions (which merely shift the Zome-path part in between in the plane but serve no further purpose regarding endpoint connectivity). To avoid nonlinearity, it could also be formulated as a special ordered set type 1 (SOS-1) constraint[4], or be omitted entirely for suitable objective functions. Moreover, note that we could assume w.l.o.g. that $x_1 = (0, 0)$ (otherwise, simply subtract x_1 from x_1 and x_2) and then may also check a priori whether x_2 even has Zometool coordinates, i.e., whether $x_2 = (\alpha_1 + \phi\beta_1, \alpha_2 + \phi\beta_2)$ with some $\alpha_i, \beta_i \in \mathbb{Z}$ for $i = 1, 2$.

   The above feasibility problem may become numerically instable because of the explicit occurrence of the golden ratio ϕ (in all but one M_i^e). However, we can make use of the special form of Zometool coordinates and, by lifting the problem into 4-dimensional space, obtain an equivalent IFP that only contains small integral coefficients. To that end, let $\hat{x} := (\alpha_1^x, \beta_1^x, \alpha_2^x, \beta_2^x) \in \mathbb{Z}^4$ be the integer representation of a point x with Zometool coordinates $x = (\alpha_1^x + \beta_1^x \phi, \alpha_2^x + \beta_2^x \phi)$. Analogously, let $\hat{M}_i^e$ be the 4×2 matrix obtained from M_i^e by replacing its columns with the respective integer representations of the corresponding Zometool coordinate vectors. Now, we can reformulate the DPC integer feasibility problem, where w.l.o.g. $x_1 = (0, 0)$,

---

[4]SOS-1$(\gamma_{e,i}^+, \gamma_{e,i}^-)$ constraints enforce that only one of $\gamma_{e,i}^+, \gamma_{e,i}^-$ may be nonzero; they can be realized, e.g., by introducing auxiliary binary variables $z_{e,i}^\pm$ and linear constraints $\gamma_{e,i}^\pm \leq \mathcal{M} z_{e,i}^\pm$ and $z_{e,i}^+ + z_{e,i}^- \leq 1$, where $\mathcal{M}$ is a sufficiently large constant (here, the respective strut budget sizes suffice, if available). Modern MIP solvers can handle SOS-1 constraints efficiently.

as:

$$
\begin{aligned}
\text{find} \quad & \gamma_{e,i}^{+}, \gamma_{e,i}^{-} \in \mathbb{Z}_{+}^{2} \quad \forall e \in \{b,r,y\}, i \in \{s,m,\ell\} & (2) \\
\text{s.t.} \quad & \sum_{e \in \{b,r,y\}} \sum_{i \in \{s,m,\ell\}} \hat{M}_i^e \left(\gamma_{e,i}^{+} - \gamma_{e,i}^{-} \right) = \hat{x}_2 \\
& \left(\; (\gamma_{e,i}^{+})_j \cdot (\gamma_{e,i}^{-})_j = 0 \quad \forall e \in \{b,r,y\}, i \in \{s,m,\ell\}, j \in \{1,2\} \; \right)
\end{aligned}
$$

Note that $|(\hat{M}_i^e)_{j,k}| \in \{0,1,2\}$ for all $e \in \{b,r,y\}$ and $i \in \{s,m,\ell\}$ ($j \in \{1,2,3,4\}$, $k \in \{1,2\}$).

Based on this integer formulation of Zome connectivity, we can, in particular, formulate the DPC variant that asks for a shortest Zome-path, i.e., one that requires the smallest number of struts to connect the given input points:

$$
\begin{aligned}
\min \quad & \sum_{e \in \{b,r,y\}} \sum_{i \in \{s,m,\ell\}} \sum_{j=1}^{2} (\gamma_{e,i}^{+})_j + (\gamma_{e,i}^{-})_j & (3) \\
\text{s.t.} \quad & \sum_{e \in \{b,r,y\}} \sum_{i \in \{s,m,\ell\}} \hat{M}_i^e \left(\gamma_{e,i}^{+} - \gamma_{e,i}^{-} \right) = \hat{x}_2 \\
& \gamma_{e,i}^{+}, \gamma_{e,i}^{-} \in \mathbb{Z}_{+}^{2} \quad \forall e \in \{b,r,y\}, i \in \{s,m,\ell\}
\end{aligned}
$$

As alluded to earlier, here, minimizing the sum of all variables (a linear function) will automatically induce the complementarity conditions $(\gamma_{e,i}^{+})_j \cdot (\gamma_{e,i}^{-})_j = 0$, which are therefore omitted.

Finally, note that strut budget restrictions can be straightforwardly integrated into all of the above models by adding constraints of the form

$$
\mathbb{1}^{\top} \gamma_{e,i}^{+} + \mathbb{1}^{\top} \gamma_{e,i}^{-} = \sum_{j=1}^{2} (\gamma_{e,i}^{+})_j + (\gamma_{e,i}^{-})_j \leq B_i^e, \tag{4}
$$

where $B_i^e \in \mathbb{Z}_+$ is the maximal allowed number of struts of color e and length i (and $\mathbb{1}$ is the all-ones vector).

3.1.2 Zome-Cycles Resembling a Shape Contour

Let us now turn to the problem of approximating a shape contour by a Zometool cycle. We handle the nontrivial task of $\mathcal{F}$-resemblance by requiring our $\mathcal{G}$-cycle to pass through the respective neighborhoods of predefined sample points along $\mathcal{F}$, i.e., we consider the DCA-S problem. Concrete options for choosing the sample points will be discussed in the next section; for now, assume they are already given.

Again, we focus on the objective of finding such a $\mathcal{G}$-cycle that consists of as few struts as possible (per segment between nodes placed in sample point neighborhoods). As mentioned before, this property can generally be seen as a loose proxy to the ultimate goal of minimizing some measure of deviation from the actual shape contour, since a good $\mathcal{G}$-cycle w.r.t. the latter will neither contain undesirable detours nor zigzagging segments, both of which are also intuitively avoided by few-strut $\mathcal{G}$-cycles.

Moreover, the basic idea for our MIP model for DCA-S builds on the DPC-IP (3): We desire (at least) one Zometool node to lie in the vicinity of each sample point (i.e., in the corresponding $\mathcal{N}_{\delta}^{\rho}(p_i)$), and require each such Zometool node to be connected by a $\mathcal{G}$-path to the Zometool node in the next sample point neighborhood encountered when moving along $\mathcal{F}$ in a fixed "direction" (clockwise or counter-clockwise). To that end, we can employ point connectivity constraints similar to those employed in the IP models discussed in Section 3.1.1. Additionally, we label the variables that determine the numbers of struts to be used by segment, and introduce new variables that pertain to the Zometool nodes to be put into each sample point neighborhood. Finally, by using two continuous coordinate variables ($g \in \mathbb{R}^2$), we can model the global shift of the Zometool construction, so that the first Zometool node can be interpreted w.l.o.g. to lie at the origin $(0,0)$. This shift is then used to constrain the Zometool nodes at the end of each $\mathcal{G}$-path ($\mathcal{G}$-cycle segment) to lie in the predefined sample point neighborhoods $\mathcal{N}_{\delta}^{\rho}(p_i)$, which we define as ℓ_{∞}-norm boxes of uniform width $\delta \geq 0$ around each respective sample point. Putting this all together yields the following MIP (with optional budget and SOS-1 constraints), where $p_1, \ldots, p_k \in \mathbb{R}^2$ are the given sample points on $\mathcal{F}$:

$$\min \quad \sum_{\kappa=1}^{k} \sum_{e\in\{b,r,y\}} \sum_{i\in\{s,m,\ell\}} \sum_{j=1}^{2} (\gamma_{e,i}^{\kappa,+})_j + (\gamma_{e,i}^{\kappa,-})_j \tag{5}$$

$$\text{s.t.} \quad \hat{x}_1 = (0,0,0,0)$$

$$-\delta\mathbb{1} \leq \big((\hat{x}_\kappa)_1 + (\hat{x}_\kappa)_2 \phi, (\hat{x}_\kappa)_3 + (\hat{x}_\kappa)_4 \phi \big) + g - p_\kappa \leq \delta\mathbb{1} \quad \forall \kappa \in [k]$$

$$\hat{x}_{(\kappa \bmod k)+1} = \hat{x}_\kappa + \sum_{e\in\{b,r,y\}} \sum_{i\in\{s,m,\ell\}} \hat{M}_i^e \Big(\gamma_{e,i}^{\kappa,+} - \gamma_{e,i}^{\kappa,-} \Big) \quad \forall \kappa \in [k]$$

$$g \in \mathbb{R}^2$$

$$\hat{x}_\kappa \in \mathbb{Z}^4 \quad \forall \kappa \in [k]$$

$$\gamma_{e,i}^{\kappa,+}, \gamma_{e,i}^{\kappa,-} \in \mathbb{Z}_+^2 \quad \forall e \in \{b,r,y\}, i \in \{s,m,\ell\}, \kappa \in [k]$$

$$\left(\sum_{\kappa=1}^{k} \Big(\mathbb{1}^\top \gamma_{e,i}^{\kappa,+} + \mathbb{1}^\top \gamma_{e,i}^{\kappa,-} \Big) \leq B_i^e \quad \forall e \in \{b,r,y\}, i \in \{s,m,\ell\} \right)$$

$$\big(\text{SOS-1}\,(\gamma_{e,i}^{\kappa,+}, \gamma_{e,i}^{\kappa,-}) \quad \forall e \in \{b,r,y\}, i \in \{s,m,\ell\}, \kappa \in [k] \big),$$

where we again abbreviate $[k] \coloneqq \{1,\dots,k\}$.

We remark that (5) may take a prohibitively long time to fully solve (i.e., compute a certifiably optimal solution or detect model infeasibility) even with state-of-the-art commercial MIP solvers like Gurobi or CPLEX. In fact, this observation already holds true for the considerably simpler DPC problem (3). It may be worth mentioning that this should generally be attributed to the respective problems' NP-hardness (cf. Section 2), not the mixed-integer programming approach itself. Nevertheless, we empirically observed that if a good ("short") solution exists, (3) is solved to optimality by modern MIP solvers very quickly (typically within a few seconds). This motivates, on the one hand, the extension from DPC to DCA-S (i.e., to (5)), and on the other hand, suggests a simple time-limit-heuristic to judge model infeasibility or (sufficient for our purposes) undesirability of possible "long" solutions: If the solution process takes more than (say) a few minutes to either find any feasible solution or one with acceptable optimality gap, terminate and declare that no good solutions exist or at least can be found quickly (within the current model parameters/design decisions). When finding relatively good solutions is not a problem, but progress stalls and it takes too long to determine exact optimality, we may of course also terminate prematurely and simply use the $\mathcal{G}$-cycle from the current best known solution. The MIP optimality gap then allows to judge how "far" from optimal the solution thus retrieved still is, i.e., how much improvement (w.r.t. the number of utilized struts) could still be possible by letting the solver continue. Often, good MIP solutions are indeed found relatively quickly, and most of the remaining solver running time is spent proving optimality (by improving dual bounds until the optimality gap is closed). Later, in Section 4.1, we will also describe an extension of the above model that is more successful on instances where the solver struggles to find a feasible solution.

Finally, it is worth noting that we also considered penalizing arclength deviation as a different objective, or in a weighted combination with the cardinality objective from (5), and furthermore considered (lower and/or upper) bounding the segment arclengths to a factor of the associated input contour segment's arclength. The arclength difference can be seen as another loose proxy for the approximation error (being small if the latter is, though not necessarily vice versa) that can be evaluated regardless of the final global positioning of the DAS-structure. While such model modifications might yield slight improvements (w.r.t. the visual perception of the resulting shape approximation quality) in some cases, at least the objective variations appear to make the MIPs significantly harder to solve, and the obtained solutions seemed more likely to lead to self-intersections ("non-planarity"). Therefore, we do not consider these modifications any further in the following.

3.2 Algorithm for Zometool Shape Contour Approximation

In order to obtain a practical method able to produce good results, two aspects remained open so far: The *(model) design decision* of how to choose appropriate sample points (and the neighborhood radius δ), and the *solution construction*, i.e., how to determine the "best" (valid) $\mathcal{F}$-resembling $\mathcal{G}$-cycle among all those sharing the same combination of struts per segment that was computed by the above MIP. (Recall that any DAS path can be rearranged without disconnecting its endpoints simply by permuting its struts/edges.) Indeed, the MIP (5) is the main "work horse" for our shape approximation method, and we combine it with shape contour sampling and optimal $\mathcal{F}$-resembling $\mathcal{G}$-cycle construction to the overall scheme outlined in Algorithm 1.

The shape contour $\mathcal{F}$ can be given, e.g., as a parametric function or implicitly via a distance function/field. Any sampling scheme naturally depends on how $\mathcal{F}$ is provided or can be accessed. In the following, we

---

Algorithm 1 Zometool Shape Contour Approximation Scheme

Input: (Zome-)DAS $\mathcal{G} = (\mathcal{V}, \mathcal{E}, \mathcal{D}, \mathcal{B})$, parameter $\delta \geq 0$, shape contour $\mathcal{F}$
Output: a shortest $\mathcal{F}$-resembling $\mathcal{G}$-cycle running through all δ-neighborhoods of all sample points
  1: obtain sample points $p_1, \ldots, p_k$ along $\mathcal{F}$
  2: set up and solve the MIP (5)
  3: **for** each segment $1, \ldots, k$ between the computed (Zometool) nodes $(g + \{x_1, \ldots, x_k\})$ **do**
  4:    obtain an approximation error minimizing sequence of the associated selected struts
  5: **return** $\mathcal{F}$-resembling $\mathcal{G}$-cycle consisting of the concatenation of segment-optimal $\mathcal{G}$-paths

---

describe a quite general setting that we also used in our implementation: distance fields and piecewise-linear $\mathcal{F}$ obtained from these. More precisely, assume we are given a (discretized) distance field covering a rectangular portion of $\mathbb{R}^2$, in the form of a matrix of values specifying the average distance of points within small square cells in 2D space (i.e., every matrix entry is the average distance value for such a cell). The size of these squares' sides is determined relative to the (shortest) strut length of the employed DAS by a scaling/accuracy parameter s, where for $s = 1$, a globally fixed ratio is used. (Thus, for $s > 1$, struts become longer relative to the input shape.) With infinite discretization precision, points lying exactly on the shape contour (boundary) would yield a distance value of zero. We assume that circle-like shapes are processed, i.e., the shape contours are closed curves that enclose exactly one connected area, so that the terms "inside" and "outside" of the shape are well-defined. Thus, cells containing points that (mostly) lie inside the shape have negative distance values, and those outside have positive distance values. Such a distance field provides a simple way to evaluate strut costs, and can also be used to obtain a polygonal approximation of the true shape by applying a 2D version of the marching cubes algorithm [16]. This approximation is what we will, for simplicity, henceforth refer to as $\mathcal{F}$; note that it is piecewise-linear and fully described by an ordered sequence of points, say $p_1^{\mathcal{F}}, \ldots, p_n^{\mathcal{F}}$.

3.2.1 Sampling the Input Shape Contour

Since the MIP (5) is oblivious to $\mathcal{F}$ beyond enforcing the placement of Zometool nodes in the vicinity of sample points, a careful selection of the sample points (which define the partition of the $\mathcal{G}$-cycle into segments) seems crucial for ensuring that the $\mathcal{G}$-cycle to be computed actually does closely resemble $\mathcal{F}$. The selection should ideally achieve a balance between several competing goals: To keep the MIP small (and therefore easier to solve), the number of segments should not be too large. However, long segments contain many struts (leading to larger effort to enumerate permutations in the final step of the overall algorithm, or decreased likelihood of a greedy scheme to work well) and the MIP objective of minimizing the number of struts will lead to strut sequences that lose resemblance to $\mathcal{F}$ (cutting off "nooks and crannies" of the contour). We found that this last aspect appears to be the most problematic, if one is willing to spend some time on the MIP optimization. Similarly, the box-radius δ for the MIP should not be set too small, lest the MIP becomes infeasible, but not too large either, since we want to ensure the $\mathcal{G}$-cycle remains close to $\mathcal{F}$ at least around the sample points.

Thus, the sampling phase of our algorithm is of a "high-level" heuristic nature; similarly, so is splitting the low-level optimization into the MIP (feasibility) part and the (optimality) part in which struts are rearranged to minimize the approximation error. Indeed, finding the optimal sample point selection is essentially equivalent to solving the entire problem, because if we knew it (and assuming δ is sufficiently large), all that would remain is finding and arranging the struts that achieve minimum approximation error. Moreover, if the sampling is "very good", the decomposition into MIP and strut-rearrangement can be expected to closely resemble what could be achieved by the abstract algorithm that could directly compute minimum approximation error solutions. (Recall that such a method is impracticable, since approximation errors can only be evaluated once strut locations are fixed.) Therefore, it is worth trying to design a sampling mechanism that targets the possibly problematic aspects mentioned above and also aims at retaining a MIP subproblem that is sufficiently tractable in practice.

We have implemented and tested the following sampling schemes:

1. *Uniformly by arclength:* Determine the (approximate) arclength a of $\mathcal{F}$ (here, the sum of the lengths of all straight lines between neighboring points $p_i^{\mathcal{F}}$). Starting with an arbitrary point, say $p_1 := p_1^{\mathcal{F}}$, pick the others by moving from the previous point along the sequence of points defining $\mathcal{F}$ until the traversed curve segment reaches the average segment arclength a/k, and select the current point in that sequence as the next respective sample point.

2. *By curvature:* For each $p_i^{\mathcal{F}}$, $i = 1, \ldots, n$, we can obtain approximate curvature information w.r.t. $\mathcal{F}$ as

$$c_i := \arccos\left(\frac{\left(p_{(i-t)_n}^{\mathcal{F}} - p_i^{\mathcal{F}}\right)^{\top}\left(p_{(i+t)_n}^{\mathcal{F}} - p_i^{\mathcal{F}}\right)}{\left\|p_{(i-t)_n}^{\mathcal{F}} - p_i^{\mathcal{F}}\right\|_2 \cdot \left\|p_{(i+t)_n}^{\mathcal{F}} - p_i^{\mathcal{F}}\right\|_2} \right),$$

which gives the angle (in radians) between the vectors connecting $p_i^{\mathcal{F}}$ with its t-th predecessor and t-th successor (in the ordered sequence defining $\mathcal{F}$), respectively, where $(j)_n$ denotes the index correctly shifted periodically back into $\{1, \ldots, n\}$, so, e.g., $(j)_n = j - n$ for $n + 1 \leq j \leq 2n$ and $(j)_n = n - j$ for $-n < j \leq 0$. Here, $t \geq 1$ can be chosen arbitrarily; $t = 1$ works, but larger values, say 5 or 10, could stabilize against tiny "kinks" in the contour that are not really relevant w.r.t. the actual shape. It holds that $c_i \in [0, \pi]$ for all i, where values close to $\pi/2$ amount to steep angles ($\pi/2$ signifies a $90°$ turn) and values close to 0 or π indicate flat regions ($0°$ or, equivalently, $180°$). For simplicity, let us define adjusted curvatures

$$\bar{c}_i := \min\{c_i, \pi - c_i\} \in [0, \pi/2];$$

note that steep angles now simply coincide with large adjusted curvature values.

As a DAS is generally better suited to approximating relatively flat curves, and (especially when minimizing the number of edges/struts that is used) indeed tends to ignore or "cut off" bends in the contour along a segment, it intuitively makes sense to take curvature information into account when selecting sample points, in an effort to reduce the occurrence of such undesirable cut-offs. We considered several different schemes based on the (adjusted) curvature values:

(a) *Global largest $\bar{c}$-values:* Pick the k points with largest $\bar{c}$-values as sample points.

(b) *Segment-wise largest $\bar{c}$-values:* First determine the segments (e.g., by arclength as described above) and then pick the k sample points as the respective points of $\mathcal{F}$ with largest (adjusted) curvature from each respective segment.

(c) *Separation-based:* Repeat picking an available point of largest $\bar{c}$-value as a sample point and marking all points in segments of arclength up to $\lambda a/k$ in both directions along $\mathcal{F}$ from this point on as unavailable, until k points were chosen. Here, $\lambda > 0$ determines how large the unsampled segments may become; e.g., aiming at equal-arclength segments, one could set $\lambda = 0.5$. (Note that overly small values of λ may lead to a bad, local concentration of the chosen sample points, whereas too large values could result in having marked all remaining points as unavailable before k sample points were chosen.)

3. *By curvature with gap-filling:* Choosing points solely based on curvature information may lead to inadequate sampling of "less curvy" segments of the input contour. This can be avoided by augmenting a separation-based curvature sampling similar to the one detailed above with a point-insertion scheme aiming at an efficient coverage of underrepresented segments with further sample points:

(a) *Separation-based with Euclidean farthest-point insertion:* Choose (up to) a fixed number k_c of sample points based on (adjusted) curvature obeying arclength separation requirements, then add more points by iteratively picking a point with maximum minimal Euclidean distance to one of the already selected sample points (up to a given maximum number k', and stopping early when the distances fall below a certain threshold).

(b) *Separation-based with arclength-based farthest-point insertion:* Again choose (up to) k_c sample points based on curvature with separation requirements, then add more points by iteratively picking a point with maximum minimal arclength distance to one of the already selected sample points (up to a given maximum number k', and stopping early when the distances fall below a certain threshold).

(Here, in (a) and (b), $k \leq k_c + k'$ then denotes the final number of adaptively selected sample points.)

Generally, the more sample points are chosen, the less pronounced the differences between the different sampling schemes become. When keeping an eye not only on the sampling quality but also on the MIP size (i.e., trying to keep it small), preliminary experiments indicated that the final curvature- and separation-based variant with arclength-based farthest-point insertion, i.e., 3(b), seems to give the visually most appealing results when using a managable number of sample points. This supports the reasoning that led us to its formulation: In addition to the points discussed at the beginning of this section, on the one hand, in "low-resolution" (large s) regimes, delicate parts of the shape contours are essentially impossible to be accurately reflected in the DAS construction, and therefore the precise location of the sample points may not be so relevant overall. Yet, it nevertheless makes sense to place some at high-curvature segments, as done by the

heuristic 3(b) (and others), in order to have the final approximation not completely ignore protruding shape parts. On the other hand, in "high-resolution" (small s) regimes, the number of sample points can naturally be increased (compared to large s settings), since the separation requirement between sampled points is less restrictive at such scales, which has two effects: First, more high-curvature segments of the input shape can be sampled, which allows to capture such critical regions more accurately. Second, further sampling by the arclength-based farthest-point insertion part of our selection heuristic 3(b) then provides a relatively even spread of sample points along the whole shape contour, and also leads to segments being "more straight", which is beneficial w.r.t. DAS representability using few struts.

Therefore, heuristic 3(b) is the sampling scheme we recommend for use in Algorithm 1 and the one employed in the numerical experiments discussed later. It should be noted that the farthest-point insertion part does add a few seconds of runtime, but this is near negligible compared to the MIP solving time and appears to be worthwhile.

3.2.2 Constructing the Zome Cycle

As already mentioned, it is up to the concrete definition of an error measure to identify the "best" sequence of struts in a $\mathcal{G}$-path. Here, we make use of the distance field that is provided as input (cf. Section 3.2.1) and employ a simple sample-averaged approximation of the area between the strut and input contour segments: For a strut e with endpoints p_1 and p_2, we compute its approximation error (cost) a_e as

$$a_e := \frac{\|p_1 - p_2\|_2}{k+2} \sum_{i=0}^{k+1} \left| d\left(\tfrac{i}{k+1} p_1 + (1 - \tfrac{i}{k+1}) p_2 \right) \right|,$$

where $d(p)$ is the value of the distance field cell containing point p. In case p lies beyond the boundaries of the given distance field, we let $d(p)$ be the value of the closest field cell multiplied with a penalty of 100. (Note that in order to avoid such penalties, the given distance field should extend sufficiently far "outside" of the shape contour.) In our numerical experiments, we use $k = 3$.

Note that, in principle, it would be possible to compute the area exactly or use exact point-to-polygon distances rather than distance field values (at least for polygonal input curves); similarly, one could refine the averaging by weighting every piece of a strut by its respective length within each distance field cell the strut passes through. However, since it already provided satisfactory results, we opted for the above-described cheaper sample-averaged area approximation that makes use of distance field values.

Note that our error measure turns out to be entirely separable (w.r.t. struts), so the total cost of a given $\mathcal{G}$-cycle C with segments $\mathcal{S}_1, \ldots, \mathcal{S}_k$ can be written as

$$a(C, \mathcal{F}) = \sum_{\kappa=1}^{k} \sum_{e \in \mathcal{S}_\kappa} a_e. \tag{6}$$

In Algorithm 1, the final step consists of constructing the actual Zome cycle using the number of struts (of each type) for each segment obtained from the MIP. To find the best permutation of struts for each segment w.r.t. the cost function defined above, we can resort to total enumeration (with some reduction of the computational effort by aborting enumeration of subsequences that are provably worse than the respective current best bound). Since this requires an undesirably long time for segments containing more than roughly 15 struts, we also implemented a greedy construction scheme which iteratively constructs the path from the segment's starting point to its end point by appending the (locally) cheapest one of the remaining struts. In our experiments, for $s \geq 2$, we usually ended up with sufficiently short (i.e., few-strut) segments to use the exact (total enumeration) construction method; nevertheless, empirically, the greedy method delivered comparable results. For $s \leq 1$, enumeration appears to typically be too expensive. As an automatic default choice in our implementation, we use total enumeration for segments containing at most 10 struts, and the greedy scheme for longer segments.

It is worth mentioning that for the purpose of our algorithm, separability w.r.t. *segments* would generally suffice, if total enumeration is employed. Then, one could still enumerate all possible realizations of each segment and evaluate some (possibly more sophisticated) segment-based approximation cost for each such realization to pick the best one. However, the separability w.r.t. struts of the above measure provides the advantage of being able to use (e.g.) our greedy scheme to avoid enumeration for segments with a number of struts that would render it prohibitively slow. Indeed, without this separability, it would apparently be much less clear how the strut arrangement could be done efficiently in such cases. In practice, this would imply that our method could typically only solve problems at lower resolutions (i.e., with larger values of the scaling parameter s), since there the number of struts in each segment turns out to be sufficiently low.

3.2.3 A Note on Simulated Annealing

Previous algorithmic work on Zometool shape approximation treated the 3-dimension problem with a simulated annealing (SA) method, see [28, 29]. Now that we have established our formal problem definitions (DCA-S, DPA-S, DPC) and described our novel three-phase algorithm, but before we delve into computational experiments, it seems appropriate to reconsider the SA idea in the present context. Besides some obvious drawbacks of this approach that have been mentioned in the introduction, SA is problematic here mainly for two reasons: First, since we prescribe only a global maximum tolerance δ around the sampled anchor points, an SA procedure would have vanishing gains for all (local improvement) moves that affect regions where the approximation error is already below the threshold. This may lead to a very high number of redundant moves that would have to be avoided by some more sophisticated meta-strategy. The second issue is that in order to obtain acceptable SA runtimes, one needs to be able to construct good starting solutions; however, it is unclear how to achieve this in our DCA-S/DPA-S setting with prescribed sample points p_i and approximation (sample point neighborhood size) tolerances δ.

In fact, the MIP solution in the main stage of our novel algorithm could be interpreted as this starting solution, and the concluding strut permutation (phase three) could be implemented as an SA procedure. However, especially since the segments typically consist of only a modest number of elements, we can just search exhaustively or apply a simpler greedy scheme. (It might be possible to further improve greedy arrangements by local improvement steps of a 1-opt or 2-opt nature, which would still be generally simpler than SA. We have not implemented such further postprocessing simply because we found the results satisfactory as is.)

As briefly mentioned earlier, while SA generally does not provide solution quality guarantees, it is admittedly true that similarly, our present approach has no theoretical guarantees in terms of the approximation error that is minimized by the strut arrangement in its final phase. The MIP solver, however, employs a branch-and-cut scheme that is, in principle, a theoretically exact method that terminates in finitely many steps. (Of course, as the problem is NP-hard, the number of iterations may still be huge, so we abort the process early after a prescribed time limit.) Also, our heuristic for the sampling phase is of course designed to allow for an eventual solution with good resemblance to the input shape, but in terms of the problem DCA-S, it may also be viewed as a means to provide (parts of) the *input* data for the problem under consideration: The choice of δ, i.e., the size of the boxes around the sampled anchor points, is another input of the MIP, and solving the MIP (5) therefore is an *exact* method for DCA-S.

4 Experiments

We implemented our algorithm in `C`, using Gurobi 9.1.1 as MIP solver; the code can be obtained from the first author's homepage[5]. The Contour Explorer plugin for Open Flipper [23] (provided by Ole Untzelmann) allowed to extract the input data (distance field, polygonal contour approximation $\mathcal{F}$) for our "ZomeDCAS" program from slices of 3D object models or based on given images (e.g., scans of handdrawn shapes); here, all test images were generated from licence-free pictures found on the internet. In each instance, the distance fields sides' have a length of 0.4 (so for $s = 1$, the shortest strut b_1 has length $2s = 2$.). The experiments were run under Linux on a quad-core machine with Intel i7-7700T CPUs (2.90 GHz, 8 MB cache) and 16 GB main memory.

We used the sampling scheme 3(b) in all experiments, requiring an arclength equivalent to the length of three longest (i.e., long blue) struts separating the points chosen based on (adjusted) curvature, and half that for the subsequent farthest-point insertion. The total number of sample points was limited to 300 (which was reached only once in all of our experiments; typically, much fewer sample points were used). In the MIP, we do employ SOS-1 constraints, and allow the solver Gurobi to run in concurrent mode on all CPU cores, each with a (wall-clock) time limit of 900 seconds. Finally, we use full strut-enumeration on segments with at most 10 struts, and the greedy scheme for longer segments, to construct the output Zome cycles with smallest approximation error. Deviations from this setup in specific experiments will be stated explicitly.

Initialization and cycle construction times combined were well below 10 seconds on most test instances (and still no more than 1 minute for large instances with small s), so the majority of the runtime is spent in MIP solving. Our program also generates tikz code to visualize the contour and Zome approximation: the respective input shape is drawn in grey (its boundary is the input contour) and Zome struts in their respective colors; the boxes around sampling points are shown as opaque dark-grey squares, the one slightly darker than the rest contains the Zome origin (best seen in the electronic version of the paper, zooming in). Note that in the Zome constructions displayed below, segments of the same color may—and often do—consist of a *sequence of struts*, not necessarily a single one; we refrained from drawing the Zome nodes

---

[5] https://www.tu-braunschweig.de/mo/team/tillmann

between struts in order not to clutter the plots. The results of our computational experiments are presented in Figures 4, 5 and 6.

Let us begin with a selection of example results of our algorithm, displayed in Figure 4. Overall, these results demonstrate that our proposed algorithm is indeed capable of obtaining good DAS/Zometool approximations of given shape contours within reasonable time, where higher resolution (smaller s) generally leads to better results since naturally, shorter struts can more accurately recreate contours. It is worth pointing out that some of the images were chosen specifically to provide a challenge for our automated algorithm pipeline (especially the sampling scheme): The shapes in Figures 4(b), (c) and (d), in particular, have both quite "curvy" parts and narrow parts. Nevertheless, the overall quality of the computed approximations allow to conclude that, all in all, our sampling scheme successfully addresses the necessity to carefully sample "curvy" regions, and that the idea of targeting few-strut representations of segments between sample point neighborhoods then provides a suitable way to induce $\mathcal{F}$-resemblance.

Moreover, this mostly also succeeds in providing strut collections that are then arranged without dramatic collision issues in regions such as the narrow parts: The worst self-intersections can be seen in the dog leash in Figure 4(b) and the staff held by the dancer in Figure 4(d), but even these at least appear to be resolvable by rearranging the struts (manually or by a, at this point hypothetical, postprocessing routine). The remaining figures, in fact, all turned out to be collision-free.

This even holds for the umbrella guy in Figure 4(c), although here the overall approximation quality is clearly not very good. This may be explained by the very low number of points that were sampled based on curvature, which supports the reasoning behind our sampling heuristic 3(b). Moreover, here, quite clearly the strut arrangements in certain segments are suboptimal (consider, e.g., the head or the part where the umbrella's shaft meets its screen), and indeed, note the comparatively large approximation error (cost) $\alpha(C, \mathcal{F})$; this is apparently due to the artificial extension of the distance field (involving penalties) used to estimate the distance/approximation error and should therefore be fixed by resorting to (more costly) actual point-to-curve-segment distances for the employed sampled area approximation. (Note also that, in general, the numerical values of approximation error may not be highly informative – surely, smaller is generally better, but half as large does not necessarily mean twice as good; ultimately, different solutions may appear more or less appealing to the beholder irrespective of the computed approximation error, so a final quality assessment has a subjective component that cannot be quantified exactly.)

Furthermore, we remark that the reported MIP optimality gaps do not pertain to the final approximation error, but show how much improvement w.r.t. minimizing the number of utilized struts could still be achieved (at most) by letting the MIP solver continue. For the experiments in Figure 4, the gaps translate to explicit lower bounds on the optimal number of struts, namely (a) 128, (b) 403, (c) 139, (d) 210, (e) 103, and (f) 273. Thus, depending on the instance, there would still be some improvements to be gained. In fact, considering that actually building a computed representation using the Zometool kit, i.e., assembling the shape approximation by following the computed "construction manual" possibly consisting of several hundred struts arranged in a certain order, would likely take a person several hours, spending more computational efforts in the MIP phase and/or to arrange struts afterwards to obtain high-quality and low-(strut-)complexity solutions would surely be justified.

As a final comment on Figure 4, let us point out that the result in Figure 4(b) was, in fact, obtained using not the full Zometool set with short, medium and long struts of the three colors. Indeed, the MIP solver failed to find a feasible solution within 900 seconds (and much longer). Thus, we took out the long struts of each color, and the presented result hence uses only short and medium struts. Obviously, it is still feasible in the full Zometool set; in fact, specific to Zometool (not arbitrary DASs), we know that for each color, the longest strut is precisely as long as the short and the medium one combined. Thus, using Zometool, there is another design choice to make: If we prefer to find Zome constructions with the fewest possible struts, the long struts must be included, because their availability allows to replace a short and a medium one (if placed after one another) and the MIP solver can decide automatically if this is advantegous and feasible. On the other hand, not using the long struts allows for a refined arrangement of the (shorter) struts in the final algorithm phase, to minimize the approximation error. Both viewpoints are compatible, since the goals of low construction complexity and low approximation error are competitive. Moreover, we could switch between using and not using long struts basically at any point: Having computed a solution without them, we can check the final outcome and replace occurrences of same-colorpairs of one short and one medium strut placed in a straight line after one another by a long strut, to reduce the strut count by (re-)introducing the long ones. For the example in Figure 4(b), one can reduce the total strut count by 3 this way, replacing one strut pair of each color by the corresponding long struts. Similarly, one could solve the MIP with the full Zometool set, and replace all occurring long struts by a short and medium one each before computing the strut arrangements that minimize the approximation error, to allow for better results there. Since these aspects seem to us like a choice that should be left to the user, we keep to the full Zometool set (always using long struts throughout our algorithm, in particular) in all further experiments.

(a) $s = 5, \delta = 8, k_c = 25 \rightsquigarrow k = 49$,
(138 struts, MIP gap 7.25%, cost $\approx$ 12026.2)

(d) $s = 2, \delta = 4, k_c = 35 \rightsquigarrow k = 79$,
(260 struts, MIP gap 19.23%, cost $\approx$ 4007.0)

(b) $s = 3, \delta = 6, k_c = 50 \rightsquigarrow k = 106$,
(422 struts, MIP gap 4.50%, cost $\approx$ 10126.83)

(e) $s = 5, \delta = 8, k_c = 25 \rightsquigarrow k = 41$,
(108 struts, MIP gap 4.63%, cost $\approx$ 10029.4)

(c) $s = 5, \delta = 5, k_c = 3 \rightsquigarrow k = 42$,
(159 struts, MIP gap 12.58%, cost $\approx$ 1543361.4)

(f) $s = 2, \delta = 4, k_c = 35 \rightsquigarrow k = 99$,
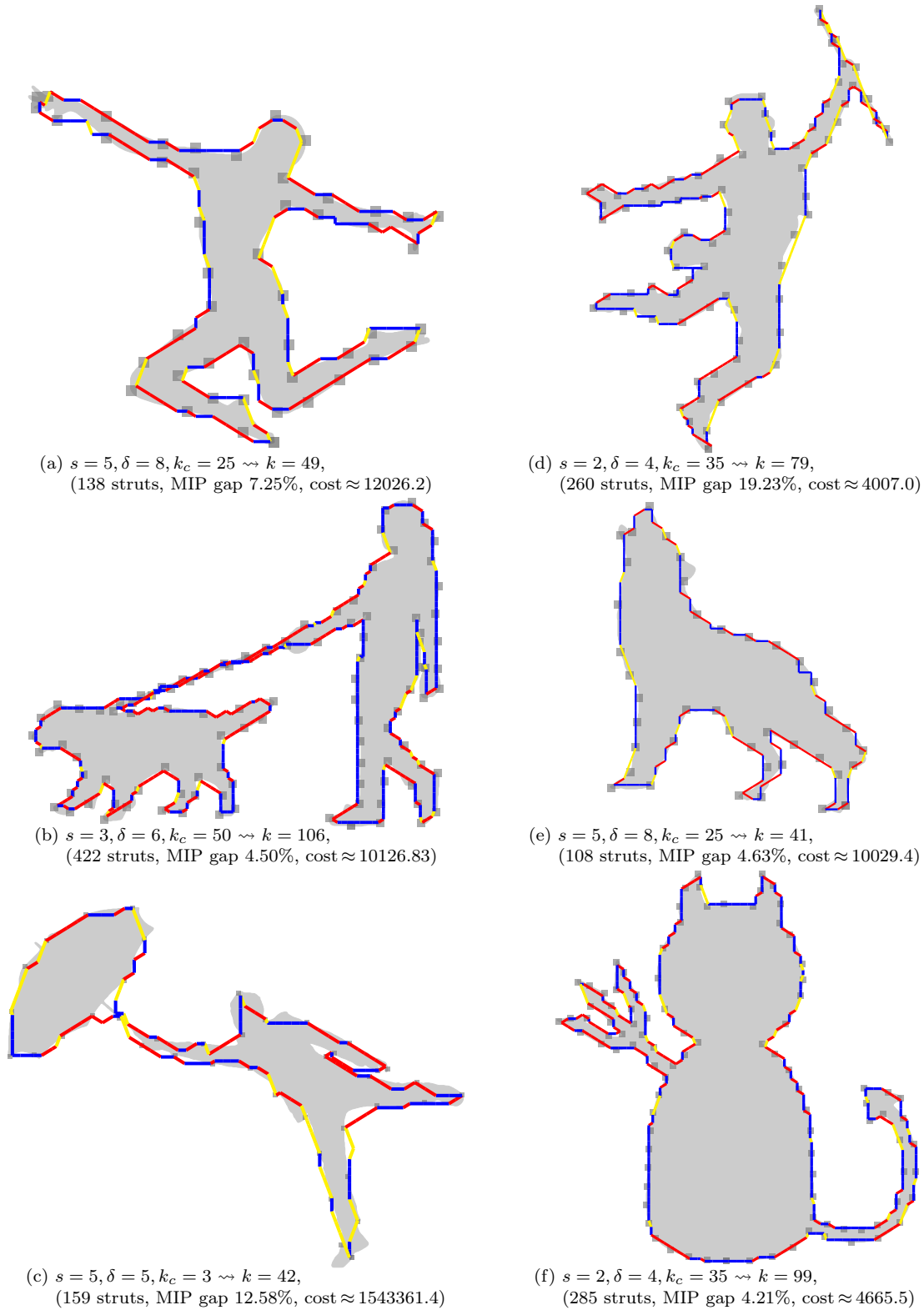(285 struts, MIP gap 4.21%, cost $\approx$ 4665.5)

Figure 4: Experimental results for various test shapes. (MIP time limit: 900 seconds).

We will provide a more structured comparison of the influence of the different solver parameters (scale s, desired approximation tolerance δ around the sample points, number k_c of points selected based on adjusted curvature, and time limit) later (cf. Figure 6 and discussion in Section 4.2 below). Before we do so, we would like to point out an aspect of our approach that turned out to be somewhat problematic when applying it in practice, namely the choice of δ (in combination with a suitable scale parameter s). Specifying some more or less arbitrary δ and s values, we quite often found that the MIP solver failed to find any feasible solution (at least within the time limit). In the next subsection, we describe this problem in a bit more detail and propose a remedy in the form of a slight relaxation of the MIP model that seems reasonable from a practical standpoint and proved to be very effective empirically.

4.1 Relaxing the Neighborhood Containment Constraints

As mentioned just above, we observed that feasibility of the MIP (5) appears to hinge somewhat crucially on the user-prescribed parameter δ, i.e., the desired approximation tolerance around the sampled anchor points on the input curve. While values $\delta > s$ usually do not seem to pose problems so often, $\delta \leq s$ implies that only a single Zome node can be placed within each sample point neighborhood, which unfortunately seems more likely to be too restrictive in the DAS construction context, as the MIP solver then fails to find even a single feasible solution within the inspected time limits. This indicates that no "nice" Zome constructions that obey the neighborhood containment constraints and allow for few-strut segments connecting them might exist in such cases. While we can observe this behavior empirically, there remains the problem that there is no clear way to identify workable pairs (δ, s) a priori. Keeping δ fixed and reducing s significantly would likely often work, but arbitarily adjusting the scale seems somewhat unintuitive. Similarly, one will likely not want to choose a very large δ, as it relates to approximation quality.

Nevertheless, recall from the beginning of Section 3 that, conceptually, respecting a global approximation tolerance δ is merely a desideratum, translated into the hard box-constraints in our MIP (5), and that our overall algorithm does not guarantee that all points along the constructed Zometool contour actually stay within distance δ of the input curve. In the practical application of our method, the user (so far) has to choose a δ-value, but as alluded to above, there is only vague intuition on how to actually make such a choice: too small a value may be too restrictive, given the relative inflexibility of discrete assembly systems to satisfy arbitrary positioning demands, while overly large values ultimately lead to cruder shape resemblance and could invite other unwanted issues such as self-intersections (e.g., when sampling point neighborhoods overlap).

Thus, we may argue that the choice of δ should not be treated as highly important, and could in fact be relaxed in order to improve flexibility of the MIP model to find suitable candidate solutions, even if they ultimately slightly violate the prescribed δ tolerance. To that end, we can extend the MIP (5) by introducing a slack variable $s_\delta \in \mathbb{R}_+$ and modifying the box-constraint bounds $\pm\delta\mathbb{1}$ to $\pm(\delta + s_\delta)\mathbb{1}$, respectively. Thus, by assigning a positive value to s_δ, the solver can automatically enlarge the neighborhoods around the sample points; since clearly, larger neighborhoods allow for the containment requirements to be met more easily, the solver can thus find Zome constructions respecting the enlarged neighborhoods more easily. In order to retain a meaningful model, the values of s_δ must of course be bounded above; indeed, we propose to additionally modify the objective function of (5) by adding a penalty term on the slack value, effectively minimizing not only the number of struts used but also the slack variable. In our implementation, we found that an objective coefficient of $10\,000$ for the slack variable seems to work quite well across scales (though this has not been thoroughly benchmarked; smaller values might work similarly well and might be better suited when the user-provided δ is really small, since otherwise, the implied priority of large coefficients to try hard to reduce the slack value would ultimately lead to insufficient enforcement of keep the Zome connections short).

This extension of our MIP model turned out to be quite effective in previously problematic δ-regimes $(\delta \leq s)$, where the solver may not find any feasible solution within up to an hour, in particular for instances with $s \leq 1$ (high resolution, and consequently, usage of comparatively many struts) but also for other settings where finding a feasible initial solution apparently challenged to solver. We note that for the slack-endowed model, longer running times are adequate in order to have the solver first reduce the slack to a sufficiently small level (if possible) that the number of struts objective eventually becomes the driving force for further optimization progress; thus, when 900 seconds often worked well for our original hard-constrained approach, we generally suggest allowing 1800 seconds for the relaxed variant.

Some example results computed with our modified algorithm are shown in Figure 5. Recall from our discussion of Figure 4(b) that the original, hard-constrained MIP (5) failed to find a feasible solution when the full Zometool construction set was used; in contrast, Figure 5(a) shows the result—using all Zome struts—when we employ the soft-constrained MIP: a solution with slack-value 0 (i.e., the desired approximation tolerance around sample points is, in fact, satisfied), significantly fewer struts, and even a lower final approximation error (cost). While there are still are some self-intersection issues along the leash, this nevertheless demonstrates that the relaxed approach can be beneficial even if the original slackless version also works. The other images in the figure all look quite well, too, with few to no (in case of the lion in Figure 5(b), and apparently also the angel (c) and even the octopus (d)) nonplanarity issues. The octopus is a very large instance, making the MIP particularly hard, so we allowed it to run for three hours; while the solver was not nearly done by that time, the intermediate result depicted in Figure 5(d) already looks very promising and the resemblance of the computed Zomecycle to an octopus is clearly there. While the slack values show that the solver gets more or less close to achieving the desired prescribed box-size δ (within the specified time limits), depending on the instance, we emphasize that the original solver without the slack variable introduced in the previous subsection did not produce any solution for any of these instances. The cost values might become quite uninformative again if the distance field is insufficient to capture all strut

(a) $s = 2, \delta = 6, k_c = 50 \rightsquigarrow k = 106$,
(268 struts, slack $= 0$, cost ≈ 9587.0)

(b) $s = 2, \delta = 2, k_c = 75 \rightsquigarrow k = 120$,
(350 struts, slack ≈ 0.01, cost ≈ 3921.0)

(c) $s = 1, \delta = 1, k_c = 100 \rightsquigarrow k = 284$,
(724 struts, slack ≈ 4.43, cost $\approx 16 \cdot 10^{20}$)

(d) $s = 0.5, \delta = 2, k_c = 150 \rightsquigarrow k = 300$,
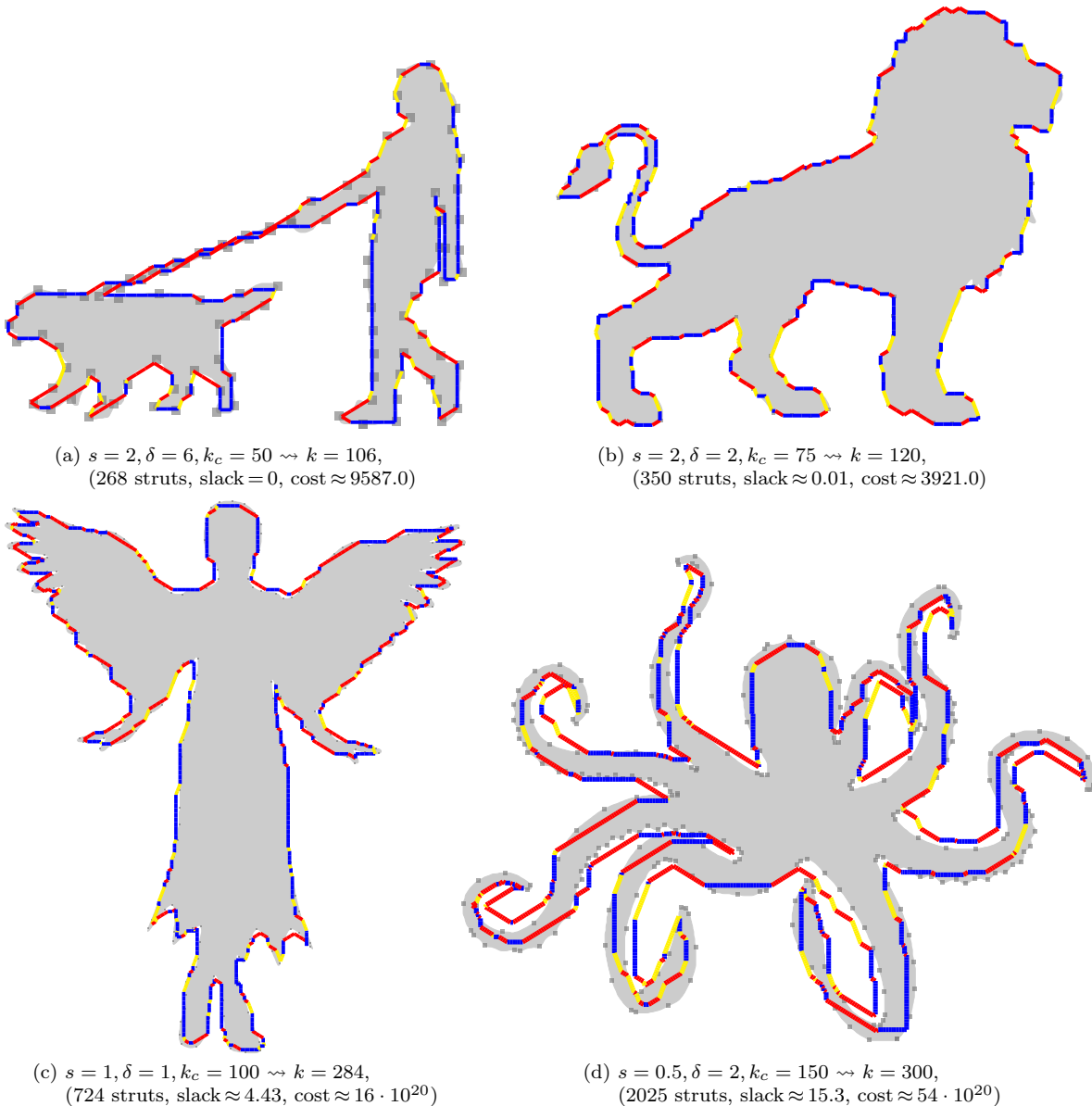(2025 struts, slack ≈ 15.3, cost $\approx 54 \cdot 10^{20}$)

Figure 5: Experimental results for the algorithm variant with relaxed MIP box constraints (MIP time limits: (a) 900 seconds, (b) 1800 seconds, (c) 3600 seconds, and (d) 10800 seconds).

parts outside of the shape, as can be seen by the huge values for the results in Figure 5(c) and (d), despite their visual quality (at least for the angel figure). As mentioned before, this can probably be ameliorated by properly extending the distance field or more expensive ways to assess strut or segment approximation errors; we leave this for future work.

4.2   Parameter Variation Experiments

The "lion" example results seen in Figure 6 highlight several aspects of the general algorithm behavior; since assessing performance changes under parameter variations with the original hard-constrained MIP variant proved cumbersome due to quite often encountering the feasibility issues described earlier, we used the slack-endowed MIP here. As a baseline to compare with, we take the result depicted in Figure 5(b).

Firstly, a higher "resolution" (corresponding to a smaller scaling parameter s) naturally allows for better shape approximation, since struts of fixed lengths can be better fitted to a relatively larger input contour than to a smaller one. This is clearly visible comparing Figure 6(a) and (d) to the baseline and to each other, especially at the chest-hair, mane, and tail parts; with the exception of the testrun using $s = 1$, where apparently the previously encountered issues with the distance field again yield a very high cost value that is quite useless, the improvement induced by using a smaller s is also reflected in the final approximation error values. Interestingly, the solver appears to make good progress on both the intuitively harder, larger instances (for smaller s) as well as on the easier ones (with larger s), so that the results reached within the

(a) $s = 1, \delta = 2, k_c = 75 \rightsquigarrow k = 225,$
(629 struts, slack ≈ 0.81, cost $\approx 10^{20}$)

(d) $s = 3, \delta = 2, k_c = 75 \rightsquigarrow k = 76,$
(240 struts, slack $= 0$, cost ≈ 6639.5)

(b) $s = 2, \delta = 2, k_c = 30 \rightsquigarrow k = 117,$
(350 struts, slack ≈ 0.08, cost ≈ 4232.8)

(e) $s = 2, \delta = 2, k_c = 120 \rightsquigarrow k = 123,$
(356 struts, slack $= 0$, cost ≈ 4175.0)

(c) $s = 2, \delta = 2, k_c = 75 \rightsquigarrow k = 120,$
(344 struts, slack ≈ 0.29, cost ≈ 3999.8)

(f) $s = 2, \delta = 2, k_c = 75 \rightsquigarrow k = 120,$
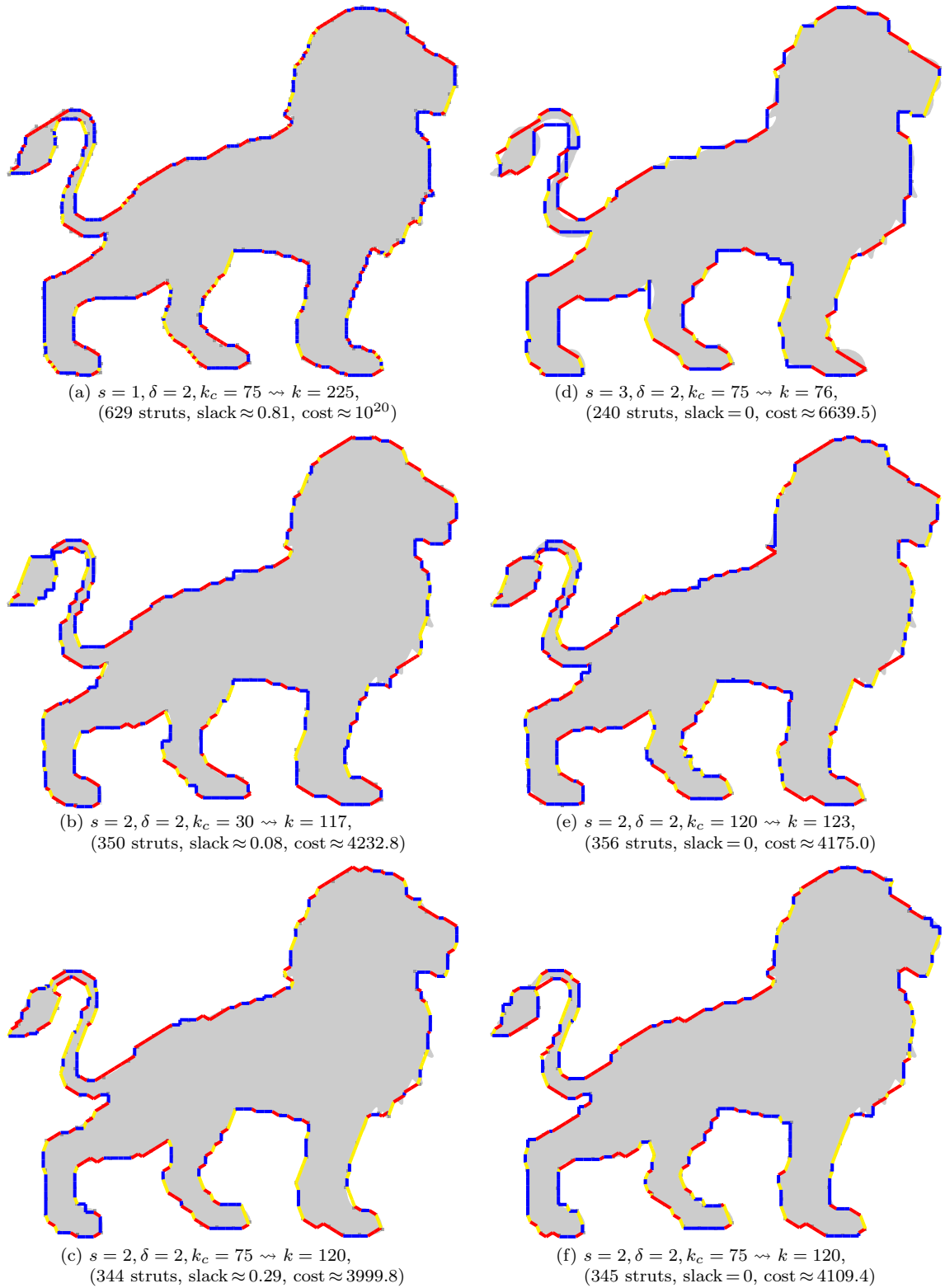(345 struts, slack $= 0$, cost ≈ 4109.4)

Figure 6: Experimental results for test shape "lion" for different algorithmic parameter choices. Baseline is Figure 5(b). Keeping all respective other parameters at their baseline values ($s = 2 = \delta$, $k_c = 75$, time limit 1800 seconds), subfigures (a) and (d) show the results for $s = 1$ and $s = 3$, (b) and (e) those for $k_c = 30$ and $k_c = 120$, (c) and (f) those for time limits 900 and 3600 seconds, respectively. The baseline and all results presented here were obtained with our algorithm using the MIP variant from Section 4.1.

same time limit of half an hour for $s = 1, 2, 3$ are all visually appealing, and with the exception of a part of the tail for the coarsest-scaling in Figure 6(d), are in fact also valid (i.e., not self-intersecting). A possible explanation for why the higher-resolution MIPs appear to not quickly become much harder to solve could be the following: Note that for smaller s, with fixed k_c, more sample points are generated using the farthest-

point insertion part of our sampling heuristic than for larger s; this is possible because of the requirement imposed in the sampling heuristics that sampled points are a multiple of the strut lengths apart, which in turn depends on s. Thus, while there are more segments and hence more variables to optimize over in the MIPs for smaller s values, the smaller s also makes it intuitively easier to meet neighborhood-containment constraints (boxes extended by the slack value must contain a Zome node) along with finding feasible strut sets to build the connections – the longer strut lengths may make this harder to achieve (and/or reduce the number of feasible options) in the larger-s regime. Nevertheless, in general, increasing s and with it, the MIP sizes, still ultimately leads to easier problems, but the result show that one does not necessarily need to plan much more time to obtain nice results at higher resolutions, too.

Next, considering Figures 6(b) and (e) (and the baseline, Figure 5(b), of course), we can see the effect of choosing more points by (adjusted) curvature before sampling the remaining uncovered segments of the input shape contour by farthest-point insertion. As it appears, here, all three images are visually quite similar, with the most noticable differences occurring at the lion's tail (probably the most critical part of the contour) and perhaps at the chest mane. Visually, regarding validity, and also w.r.t. the final approximation cost, the baseline selection k_c stands out as the best choice here. This can be explained, and provides a loose guiding principle, as follows: Due to the separation requirement of sample points, it is conceivable that there is an (instance-specific) "sweet spot", i.e., a number k_c of points to be sampled by curvature – choosing fewer by curvature, the remaining farthest-point insertion sampling can then miss more important "curvy" segments of the input curve (resulting in undesired simplification of such segments in the output), while choosing too many by curvature can lead to a number of points being sampled that are actually not of particular relevance any more (resulting in less evenly distributed sampling along less critical contour segments, which in turn can adversely affect the output approximation quality). While the best choice of k_c will certainly depend on the actual input shape (and, naturally, also to the scaling s, since for large s, fewer points can be sampled overall), a rule of thumb could be to try for a number k_c that will be roughly half the total number of sampled points. A further possibility that may be worth investigating in future work is to endow the sampling heuristic with a threshold on the curvature, to stop sampling by curvature and switch to farthest-point insertion as soon as the remaining (adjusted) curvature values fall below this threshold value.

Finally, visually comparing the results in Figure 6(c) and (f) with the baseline Figure 5(b), we note that using a shorter time limit (here, 5 minutes versus the baseline 30) can still produce similarly good solutions, using slightly fewer struts with a bit more slack and slightly worse approximation error. However, this needs not be the case for other instances. Generally, letting the MIP run for longer will of course produce solutions with smaller slack (if possible) and fewer or more struts, depending on the objective coefficient (and size) of the slack variable – larger objective contribution of the slack variable put more emphasizes on driving it down, possibly at the expense of using more struts, while once the slack has been reduced sufficiently far, the emphasizes shifts to searching for shorter Zome paths. In the present case, the slack can be reduced to zero within (less than) an hour, and while MIP optimality has not been proven after one hour (so improvements in terms of the number of struts might still be possible), the final solution now uses a few struts less than the baseline, resulting in a slight increase in the final approximation error. This can be seen as further supporting our earlier argument that a truly good a-priori selection of the desired global approximation tolerance, or sample point neighborhood size, δ is not really available, and one should therefore allow the solver to aim for the prescribed δ but not force it to reach it.

5 Concluding Remarks

While it is often achieved automatically, having no *guarantee* that edge (or node) overlaps are avoided is a present drawback of our method. Node collisions (i.e., placing two DAS nodes on top of one another) could be avoided a priori by ensuring that the neighhorhoods $\mathcal{N}_\delta^\rho(p_i)$ are disjoint, either by reducing δ accordingly or by modifying pairs of overlapping neighhorhoods directly. To disentangle edge collisions, the strut enumeration procedure, i.e., the last phase of our Algorithm 1, can be extended to be "planarity-aware". For instance, we could integrate a postprocessing procedure that tries to automatically detect and repair collisions by suitably rearranging struts, ideally aiming at keeping the increase in approximation error to a minimum. A very simple way to do this, and that can easily be seen to locally guarantee resolution of the collision, would be to rearrange the struts of the affected two $\mathcal{G}$-path/cycle segments so that the segments "bend away from each other". (Globally, this could introduce new collisions and thus might have to be iterated; it also may fail entirely and, as mentioned before, there may be cases that actually cannot be fixed at all.) We leave the details of a good (in terms of approximation error) and efficient realization of these matters for future work. As an immediate fix, one could focus on the scale: If s and δ are chosen sufficiently small (depending on the input contour resolution/scale), then one can guarantee that every sample point neighborhood contains just one DAS node, and, more importantly, provided there are sufficiently many

sampling points, minimization of the number of struts leads to relatively straight $\mathcal{G}$-segments that should be very unlikely to intersect. However, it is of course desirable to find answers to this problem that apply at coarser scales as well.

Given that the DAS setting allows only certain angles between the struts, it is conceivable that including a global rotation (of the input shape) in the optimization could yield even better results than what we achieved here using a fixed global orientation. This could, in principle, be integrated into the MIP (5) by (left-)multiplying each sample point $p_k \in \mathbb{R}^2$ by a rotation matrix

$$R_\theta = \left(\begin{array}{cc} \cos(\theta) & -\sin(\theta) \\ \sin(\theta) & \cos(\theta) \end{array} \right),$$

with variable $\theta \in [0, \pi]$ representing the (counter-clockwise) rotation degree. However, the nonlinearities introduced by the sine and cosine functions would further complicate the MIP. To keep things linear throughout, one could discretize the range for θ, or perhaps restrict to just a few selected angles such as those occurring in the DAS. A simpler, heuristic alternative to such MIP extensions could be to try to estimate a suitable global rotation a priori; for polygonal input shapes, one might, for instance, determine average angles of the input contour's line segments (maybe weighted by segment lengths) and from that determine a rotation angle so that the DAS orientations align better with more input contour parts. (One could also manipulate polygonal contours directly, changing angles to more desirable ones; a work in this direction can be found in the squaring of buildings for cartography applications [15].)

As mentioned in the introduction, we ultimately hope to extend the methodology proposed in this paper to the task of 3D shape approximation. Our algorithm constitutes the first important step in towards this goal. An idea to achieve the extension is to slice a given 3D object and use the general scheme introduced here to obtain DAS approximations of these slices along with DAS connections between them. To that end, note that our method can be straightforwardly extended to handle "chords" and "protrusions" of the input shape (i.e., curve segments that either connect two points of the main contour or lead from the contour to a point outside of it). If, for instance, the crucial points (where a chord or protrusion "leaves" the main contour) could be identified (automatically) and selected as required sample points, the new elements can indeed be incorporated into the MIP by additional point-connectivity constraints of the same kind as used in the present work to ensure $\mathcal{F}$-resemblance. How this identification could be realized in practice will likely depend strongly on how exactly the input shape is provided/represented. An alternative approach could be to first solve the problem for the main contour, and then sequentially include chords by finding DAS connections between the already-placed nodes closest to the end points of the chords (and similarly for protrusions). Once the method can handle these extensions, the "slicing" idea can be realized by using the concept of chords to enforce connections between the different DAS slice approximations, either in a sequential manner or in a single large MIP (note that moving from 2D to 3D coordinates is straightforward). It will be interesting to see how this envisioned extension will work in practice for the 3D shape approximation tasks we have in mind.

Acknowledgements

References

[1] P. K. Agarwal and S. Suri, "Surface approximation and geometric partitions," *SIAM J. Comput.*, vol. 27, pp. 1016–1035, 1998.

[2] M. G. ao, J. Krukar, M. Nöllenburg, and A. Schwering, "Route Schematization With Polygonal Landmarks," EarthArXiv preprint, 2019.

[3] E. M. Arkin, J. S. B. Mitchell, and C. D. Piatko, "Bicriteria shortest path problems in the plane," in *Proc. 3rd Canad. Conf. Comput. Geom.*, 1991, pp. 153–156.

[4] Q. W. Bouts, I. Kostitsyna, M. van Kreveld, W. Meulemans, W. Sonke, and K. Verbeek, "Mapping Polygons to the Grid with Small Hausdorff and Fréchet Distance," in *Proc. ESA*, 2016, pp. 22:1–22:16.

[5] K. Buchin, W. Meulemans, A. Van Renssen, and B. Speckmann, "Area-Preserving Simplification and Schematization of Polygonal Subdivisions," *ACM Trans. Spatial Algo. Sys.*, vol. 2, no. 1, p. Art. No. 2, 2016.

[6] D. Z. Chen, O. Daescu, and K. S. Klenk, "On Geometric Path Query Problems," *Int'l J. Comput. Geom. Appl.*, vol. 11, no. 06, pp. 617–645, 2001.

[7] S. Cicerone and M. Cermignani, "Fast and Simple Approach for Polygon Schematization," in *Proc. ICCSA*, 2012, pp. 267–279.

[8] T. Davis, "The Mathematics of Zome," available online at www.geometer.org/mathcircles/zome.pdf, 2007.

[9] M. R. Garey and D. S. Johnson, *Computers and Intractability. A Guide to the Theory of NP-Completeness.* W. H. Freeman and Company, 1979.

[10] L. J. Guibas, J. E. Hershberger, J. S. B. Mitchell, and J. S. Snoeyink, "Approximating polygons and subdivisions with minimum link paths," in *Proc. 2nd International Symposium on Algorithms (ISA'91)*, ser. Lecture Notes in Computer Science, W. L. Hsu and R. C. T. Lee, Eds. Berlin, Heidelberg: Springer, 1991, vol. 557, pp. 151–162.

[11] G. W. Hart and H. Picciotto, *Zome Geometry.* Key Curriculum Press, 2001.

[12] J. E. Hershberger and J. S. Snoeyink, "Computing minimum length paths of a given homotopy class," *Comput. Geom.*, vol. 4, no. 2, pp. 63–97, 1994.

[13] I. Kostitsyna, M. Löffler, V. Polishchuk, and F. Staals, "On the complexity of minimum-link path problems," in *32nd International Symposium on Computational Geometry (SoCG)*, ser. Leibniz International Proceedings in Informatics, S. Fekete and A. Lubiw, Eds., vol. 51. Germany: Schloss Dagstuhl – Leibniz-Zentrum für Informatik, Dagstuhl Publishing, 2016, pp. 49:1–49:16.

[14] M. Löffler and W. Meulemans, "Discretized Approaches to Schematization," in *Proc. CCCG*, 2017, pp. 220–225.

[15] I. Lokhat and G. Touya, "Enhancing building footprints with squaring operations," *J. Spat. Inf. Sci.*, vol. 13, pp. 33–60, 2016.

[16] W. E. Lorensen and H. E. Cline, "Marching cubes: A high resolution 3D surface construction algorithm," in *Proc. SIGGRAPH.* New York: ACM, 1987, pp. 163–169.

[17] W. Meulemans, "Similarity measures and algorithms for cartographic schematization," Ph.D. dissertation, TU Eindhoven, 2014.

[18] J. S. B. Mitchell, "Shortest Paths and Networks," in *Handbook of Computational Geometry,* 3rd ed. (to appear), J. E. Goodman, J. O'Rourke, and C. D. Tóth, Eds. CRC Press, Boca Raton, FL, 2017, pp. 811–848.

[19] J. S. B. Mitchell, C. D. Piatko, and E. M. Arkin, "Computing a shortest k-link path in a polygon," in *Proc. 33rd Ann. Symp. Found. Comput. Sci.* IEEE, 1992, pp. 573–582.

[20] J. S. B. Mitchell and V. Polishchuk, "Minimum-perimeter enclosures," *Inf. Process. Lett.*, vol. 107, no. 3–4, pp. 120–124, 2008.

[21] J. S. B. Mitchell, V. Polishchuk, and M. Sysikaski, "Minimum-link paths revisited," *Comput. Geom.*, vol. 47, no. 6, pp. 651–667, 2014.

[22] J. S. B. Mitchell, G. Rote, and G. Woeginger, "Minimum-link paths among obstacles in the plane," *Algorithmica*, vol. 8, no. 1, pp. 431–459, 1992.

[23] J. Möbius and L. Kobbelt, "OpenFlipper: An Open Source Geometry Processing and Rendering Framework," in *Curves and Surfaces*, ser. Lecture Notes in Computer Science, J.-D. Boissonnat, P. Chenin, A. Cohen, C. Gout, T. Lyche, M.-L. Mazure, and L. Schumaker, Eds. Berlin, Heidelberg: Springer, 2012, vol. 6920, pp. 488–500, Program code and website: www.openflipper.org.

[24] B. J. Nilsson, T. Ottmann, S. Schuierer, and C. Icking, "Restricted orientation computational geometry," in *Data structures and efficient algorithms: Final Report on the DFG Special Joint Initiative*, ser. Lecture Notes in Computer Science, B. Monien and T. Ottmann, Eds. Berlin, Heidelberg: Springer, 1992, vol. 594, pp. 148–185.

[25] M. Nöllenburg and A. Wolff, "Drawing and labeling high-quality metromaps by mixed-integer programming," *IEEE Trans. Visual. Comput. Graphics*, vol. 17, no. 5, pp. 626–641, 2011.

[26] C. D. Piatko, "Geometric Bicriteria Optimal Path Problems," Ph.D. dissertation, Cornell University, Ithaca, NY, USA, 1993.

[27] G. Reich, "Finitely-oriented shortest paths in the presence of polygonal obstacles," Institut für Informatik, Universität Freiburg, Germany, Tech. Rep. Bericht 39, 1991.

[28] H. Zimmer and L. Kobbelt, "Zometool Rationalization of Freeform Surfaces," *IEEE Trans. Vis. Comput. Graph.*, vol. 20, no. 10, pp. 1461–1473, 2014.

[29] H. Zimmer, F. Lafarge, P. Alliez, and L. Kobbelt, "Zometool Shape Approximation," *Graph. Models*, vol. 76, no. 5, pp. 390–401, 2014, Special Issue "Geometric Modeling and Processing 2014".